Title: Neuromedin U alters bioenergetics and expands the cancer stem cell phenotype in HER2-positive breast cancer

Authors: Vanesa G. Martinez[1], John Crown[2], Richard K. Porter[3] and Lorraine O'Driscoll[1*]

Affiliations: [1]School of Pharmacy and Pharmaceutical Sciences & Trinity Biomedical Sciences Institute, Trinity College Dublin; [2]Department of Medical Oncology, St. Vincent's University Hospital, Dublin 4; [3]School of Biochemistry and Immunology, Trinity Biomedical Sciences Institute, Trinity College Dublin, Dublin 2, Ireland.

[1]**Corresponding author:** Lorraine O'Driscoll, School of Pharmacy and Pharmaceutical Sciences & Trinity Biomedical Sciences Institute, Trinity College Dublin, Dublin 2, Ireland. Telephone: +353-1-8962822 Fax: +353-1-8962810 Email: lodrisc@tcd.ie

Short title: Neuromedin U and cancer stem cells

Keywords: Neuromedin U; master regulator; drug-resistance; bioenergetics; cancer stem cell phenotype

List of abbreviations

ALDH1: aldehyde dehydrogenase 1, **CSC:** cancer stem cell, **DCA:** dichloroacetic acid, **ECAR:** extracellular acidification rate, **EMT:** epithelial-to-mesenchymal transition, **NAO:** nonyl acridine orange, **NmU:** neuromedin U, **OCR:** oxygen consumption rate

Novelty and impact

NmU is known to affect energy homeostasis and metabolic rate when administered systemically, but here we established that it induces aberrant metabolism and bioenergetics at the cellular level. Metabolic abnormalities are a prerequisite for stemness. We discovered that ectopic or induced overexpression of NmU increased stemness, suggesting that NmU is a master regulator of the cancer stem cell phenotype. Targeting NmU may reduce expansion of the stem cell population, which are notoriously resistant to treatment.

Abstract

Neuromedin U (NmU) is a neuropeptide belonging to the neuromedin family. Recently, we reported a significant association between NmU and breast cancer, particularly correlating with increased aggressiveness, resistance to HER2-targeted therapies and overall significantly poorer outcome for patients, although the mechanism through which it exerts this effect remained unexplained. Investigating this, here we found that ectopic over-expression of NmU in HER2-positive breast cancer cells induced aberrant metabolism, with increased glycolysis, likely due to enhanced pyruvate dehydrogenase kinase activity. Similar results were observed in HER2-targeted drug-resistant cell variants, which we had previously shown to display increased levels of NmU. Overexpression of NmU also resulted in upregulation of epithelial-mesenchymal transition markers and increased IL-6 secretion which, together with aberrant metabolism, have all been associated with the cancer stem cell (CSC) phenotype. Flow cytometry experiments confirmed that NmU-overexpressing and HER2-targeted drug-resistant cells showed an increased proportion of cells with CSC phenotype ($CD44^+/CD24^-$). Taken together, our results report a new mechanism of action for NmU in HER2-overexpressing breast cancer that enhances resistance to HER2-targeted drugs through conferring CSC characteristics and expansion of the CSC phenotype.

Introduction

Cancer cells have different bioenergetic requirements than normal cells. As they often grow at faster rates they not only need to transduce energy at a greater rate, but also need increased numbers of building blocks to support cell proliferation. A common observation in cultured cancer cells is a switch in the habitual ATP source from oxidative phosphorylation (carried out in the mitochondria) to glycolysis. Although glycolysis is less efficient for generating ATP, the intermediate compounds produced can then be incorporated into biosynthetic pathways [1-2]. Thus, cancer cells have a tendency to have increased glycolytic flux, increased lactic acid production and increased lactic acid efflux, even under aerobic conditions, a phenomenon known as the Warburg effect. Aberrant metabolism is an emerging hallmark of cancer cells and recent studies have also shown a strong link between glycolytic metabolism and the cancer stem cell (CSC) phenotype [reviewed in [3]].

Neuromedin U (NmU) is a peptide associated with a range of different physiological functions, from smooth muscle contraction to blood pressure regulation and bone remodelling [4-5]. NmU functions have been related to energy homeostasis, feeding, core body temperature and metabolic rate regulation. Many of these studies have been performed *in vivo* and involved analysing the effect of systemic NmU levels in laboratory animals. To our knowledge, the effects of NmU on metabolism at the cellular level have not yet been studied.

A limited number of studies to date have associated NmU with cancer, with conflicting observations depending on the cancer type [4-5]. In HER2-positive breast cancer, we have shown that NmU expression is increased in cells with both innate and acquired resistance to HER2-targeted therapies; furthermore, NmU overexpression was also associated with increased migration, invasion and resistance to *anoikis* [6]. Conversely, we reported that inhibition of NmU expression by shRNA increased sensitivity to HER2-targeted therapies. In assessing data from approximately 3,500 breast tumours, our work identified an association between NmU expression and poor survival outcome for breast cancer patients, particularly those with HER2-overexpressing tumours. Our *in vitro* and *in vivo* NmU knock-down experiments pointed to a role for NmU as a new therapeutic target to help circumvent

innate and acquired drug resistance, although other adverse events associated with NmU's action remained unexplained.

Here we show, for the first time, that NmU overexpression correlates with altered cell bioenergetics, epithelial to mesenchymal transition (EMT) and increased levels of IL-6, all of which are phenotypical characteristics associated with CSCs. As expected, therefore, we also show that NmU overexpression results in expansion of the cancer stem cell (CSC) phenotype within the population. These results point to a novel role for NmU as a master regulator of the CSC phenotype and a potential target for new therapies for HER2-overexpressing breast cancer.

Materials and methods

Cell culture and treatments

HCC1954 (termed HCC1954 Par/Parent cell line here) and SKBR3 (termed SKBR3 Par/Parent cell line here) cells, obtained from ATCC, were cultured in RPMI-1640 (Sigma-Aldrich) supplemented with 10% FCS (PAA) and 1% L-glutamine. HCC1954 and SKBR3 NmU and mock-transfected cells, as well as lapatinib-resistant (HCC1954 LR), neratinib-resistant (HCC1954 NR and SKBR3 NR), and trastuzumab-resistant (SKBR3 TR) cell variants, have been previously described [3]. For short-term treatment with NmU peptide, cells (1×10^5 cells) were seeded in a 24-well plate, allowed to attach overnight, fed with serum-free medium and subsequently treated with 1-10 μmol/L of NmU-25 (Bachem) for 1 h. Cell lines were authenticated by short tandem repeat profiling and tested for *Mycoplasma* quarterly. Lapatinib and neratinib were purchased from Sequoia Chemicals Ltd. Tocilizumab was obtained from the pharmacy at St. James' hospital/TCD. LLL12 was obtained from Calbiochem.

Measurement of bioenergetics parameters by the Seahorse Extracellular Flux Analyser

The metabolic rate of cells was analysed using a Seahorse XF24 Analyser (XF24-3, Seahorse bioscience). Assays were performed according to manufacturers' instructions. Briefly, cells were seeded at $4x10^4$/well in a 24-well XF microplate (Seahorse Biosciences). When cells

were to be subjected to 72 h treatments, initial seeding cell density was $2x10^4$/well. On the day of the assay, cells were washed and 525µl of assay medium supplemented with 10mM D-(+)-glucose were added to each well. Specific inhibitors were prepared for sequential addition at the appropriate concentrations (oligomycin A, 1µg/ml; FCCP, 300µM; rotenone, 1µM; antimycin A, 1µM; and 2-deoxy-D-glucose, 30mM, all from Sigma) in XF assay medium supplemented with 10mM D-(+)-glucose. When treatment was performed with oligomycin and FCCP only, that is stated in the text.

After the Seahorse run was complete, the 24-well XF plate was recovered and the cells collected for protein isolation and quantification. Oxygen consumption rate (OCR) and extracellular acidification rate (ECAR) readings were normalised using these protein concentrations. Parameters calculated from OCR and ECAR readings are explained in graphic form in Supplementary Figure 1.

Immunoblotting

Total cellular proteins (30–40 µg for cell lysates, depending on the specific protein abundance but constant for any given protein) were resolved on 10% SDS-PAGE and transferred to polyvinylidene difluoride membranes (Millipore). Primary antibodies used included ALDH1 (BD Biosciences), E-Cadherin, β-catenin (both from Cell Signaling Technology), vimentin and β-actin (both from Sigma-Aldrich). Membranes were incubated with appropriate horseradish peroxidase-conjugated secondary antibodies (Cell Signaling Technology) and proteins were visualised by chemiluminescence (Millipore). Detection was performed with a Chemidoc exposure system (Bio-Rad Laboratories).

Wound-healing assay

HCC1954 cell variants (1.5×10^5/well) were seeded in 24-well plates and cultured for 24 h to confluency. Monolayer was scratched with a pipette tip and the resulting wounded areas were monitored by phase contrast microscopy. After a further 24 h, the rate of wound closure determined using NIH ImageJ software. Anti-IL-6 receptor antibody (Tocilizumab), when used, was added to fresh medium just before wound scratching.

ELISA

ELISA kits for human IL-6 (Peprotech), TGFβ (R&D Systems) and NmU (Peninsula Laboratories) were used according to the manufacturer's instructions. For conditioned medium analysis, HCC1954 and SKBR3 cell variants were seeded at $1x10^5$/well in a 24-well plate and left to attach overnight. The following day, cells were washed and fed with serum-free medium and incubated for a further 72 h. Supernatants were then collected and analysed immediately or stored at -80°C until analysis. Results were normalised to total cell protein contained in the respective wells.

Flow cytometry

For mitochondrial membrane potential analysis, HCC1954 cell variants cells were seeded at $1x10^5$/well of a 6-well plate and were allowed to attach overnight. Cells were then trypsinised, washed in PBS, re-suspended and incubated in 1ml of 10μM Nonyl Acridine Orange (NAO, Molecular Probes, Cat. #: A1372) in 5% FCS in PBS for 10 mins in the dark. Unstained cells were incubated in 5% FCS in PBS for 10mins. Cells were subsequently centrifuged at 2000g for 5 mins at 25°C, washed twice in PBS, re-suspended in 200μl PBS and transferred to flow cytometer tubes. Cell staining for NAO was measured using a FACSCanto II flow cytometer (BD Biosciences) and analysed using BD FACSDiva software.

For CSC phenotype analysis, HCC1954 and SKBR3 cell variants ($1x10^6$/well) were seeded in a 6-well plate and allowed to attach overnight. They were then trypsinised, blocked with 10% FCS in PBS and stained with APC-conjugated anti-CD24 (1:75) and FITC-conjugated anti-CD44 (1:800 for HCC1954, 1:400 for SKBR3) for 30 min at 4°C. Staining was assessed in a FACSCanto II flow cytometer, followed by analysis with BD FACSDiva software.

For sorting of cells with CSC phenotype, HCC1954 cells ($2.5x10^6$) were stained with anti-CD24 and anti-CD44 as before and separated in a FACSAria cell sorter. Sorted cells (CSC and non-CSC) were seeded at $1x10^5$/well in a 24-well plate for further analysis.

Statistical analysis

Two-tailed Student's unpaired t-test was used to compare two groups. Statistical analyses were performed using GraphPad Prism 5 (GraphPad Software, Inc., San Diego, CA, USA). Results are expressed as mean of a minimum of three independent experiments ± SEM. Statistical significance was set at *$p<0.05$; **$p<0.01$; ***$p<0.001$.

Results

NmU overexpression induces altered cell bioenergetics

NmU has been ascribed numerous functions in the body, among them roles in feeding, energy homeostasis, core body temperature and metabolic rate [4-5]. We therefore speculated that overexpression of NmU could alter the bioenergetics of HER2-positive breast cancer cells. To evaluate this, metabolic parameters were analysed in mock-transfected or NmU-overexpressing HCC1954 and SKBR3 cells. Basal cellular oxygen consumption rates (OCR) (mitochondrial plus non-mitochondrial) were measured using a Seahorse XF24 flux analyser and showed that HCC1954 NmU-overexpressing cells displayed significantly lower cellular OCR than control transfected cells, while there appeared to be no difference between NmU-overexpressing and control transfected SKBR3 cells (Fig. 1). Addition of oligomycin, an inhibitor of the ATP synthase, reduced the OCR in both variants, demonstrating that NmU- and mock-transfected cells have active mitochondria. Subsequent addition of the uncoupler FCCP gives a measure of maximal mitochondrial activity and in both HCC1954 NmU- and mock-transfected cells this was not found to be greater than the basal activity, suggesting that mitochondria are working at maximal activity under basal conditions. On the other hand, SKBR3 cells did increase their respiration further, indicating that their mitochondria are not typically working at maximal levels. The subsequent addition of antimycin A inhibits mitochondrial oxygen consumption, thus the OCR recorded following addition of this compound is due to non-mitochondrial oxidative phosphorylation. Clearly, there is approximately twice as much non-mitochondrial oxygen consumption in HCC1954 mock-transfected cells compared to NmU-transfected cells, while no changes were observed in SKBR3 cells. The data thus demonstrate that NmU overexpression decreases cellular oxygen consumption of both mitochondrial and non-mitochondrial origin in HCC1954, although it does not appear to affect respiration in the SKBR3 cell line.

Interestingly, the decreased steady-state OCR in HCC1954 NmU-transfected cells compared to mock-transfected cells was not associated with a concomitant increase in glycolysis, as

shown by the extracellular acidification rate (ECAR), an index of glycolysis (Fig. 2*a* and 2*c*). In fact, the ECAR was actually decreased in HCC1954 NmU-overexpressing cells compared to mock-transfected cells, with significant decreases in different ECAR parameters such as basal and maximal ECAR (glycolytic capacity). However, there was an increase in ECAR for both HCC1954 NmU- and mock-transfected cells following addition of oligomycin and a decrease in ECAR on addition of FCCP, as expected, suggesting that glycolysis is functional in both cell lines. As a result of these bioenergetics changes, the OCR/ECAR ratios were decreased in NmU-overexpressing cells, mostly due to the reduction in OCR, although the decrease was only significant in the case of maximal rates (Fig. 2*e*). These results cannot be ascribed to differences in proliferation rates, as their proliferation rates did not differ significantly (data not shown). The results were quite different for SKBR3 NmU-overexpressing cells, which showed a marked increase in glycolysis (Fig. 2*b* and *c*). Despite these differences, the overall result of NmU overexpression was a decrease in OCR/ECAR ratios, just as had been observed for HCC1954 cells. These results suggest that despite varying effects of NmU overexpression in the bioenergetics profiles of different HER2-positive cell lines, high levels of NmU are correlated with a switch to glycolysis.

To assess whether the decrease in mitochondrial respiration in HCC1954 NmU-overexpressing cells was due to mitochondrial dysfunction, we measured mitochondrial membrane potential using nonyl acridine orange (NAO). NAO is a lipophilic cation that accumulates and fluoresces in the mitochondrial matrix at high membrane potentials and thus can be used as a measure of the magnitude of the membrane potential [7]. As shown in Supplementary Figure 2*a*, overexpression of NmU did not result in any appreciable changes in NAO staining, suggesting that increased levels of NmU do not cause alterations in mitochondrial membrane potential.

NmU is secreted into the extracellular medium, acting in an autocrine/paracrine fashion on the secreting cell and others surrounding it. To evaluate the possible effects of secreted NmU, HCC1954 cells were treated with the exogenous peptide (1 μM) for 72 h before bioenergetics assessment using the Seahorse XF24. As shown in Supplementary Figure 3*a* and 3*b*, short-term treatment with the NmU peptide significantly increased the basal and maximal ECAR, while causing no appreciable change in the OCR. Interestingly, treatment with NmU also caused significant decreases in whole cellular OCR/ECAR ratios, just as had

happened with NmU overexpression in cells (Suppl. Fig. 3*c*). These results show that short-term exposure to NmU does not appear to affect mitochondrial function but is sufficient to induce metabolic alterations in glycolysis.

In order to find out more about the mechanism through which NmU induces these metabolic alterations, HCC1954 cells were treated with dichloroacetic acid (DCA) before carrying out metabolic analysis. DCA is an inhibitor of the key enzyme pyruvate dehydrogenase kinase. This enzyme can inactivate pyruvate dehydrogenase, the main function of which is to provide substrates for mitochondrial respiration. Inhibition of pyruvate dehydrogenase kinase thus increases the availability of substrates for mitochondrial respiration and stimulates this process. As shown in Figure 3*a*, treatment of mock-transfected cells with DCA did not result in any observable changes in the OCR. However, HCC1954 NmU-overexpressing cells significantly increased their OCR and all associated parameters following DCA treatment (Fig. 3*c*), suggesting that pyruvate dehydrogenase kinase activity is at least partly responsible for the observed decrease in OCR in these cells. Treatment with DCA did not significantly affect ECAR in mock-transfected or NmU-overexpressing cells (Figs. 3*c* and *d*).

IL-6 has been termed the endocrine cytokine, as it appears to be involved in processes related to energy, feeding and metabolism [8]. These studies have been performed *in vivo*, in laboratory animals and healthy or diabetic humans treated systemically with IL-6 but, to the best of our knowledge, the effects of IL-6 in cancer cell metabolism have not been studied at the cellular level. To assess the contribution of IL-6 signalling to bioenergetic alterations in HCC1954 NmU-overexpressing cells, treatment with LLL12, an inhibitor of STAT3 –a downstream mediator of IL-6 signalling– was performed prior to metabolic analysis. Inhibition of IL-6 signalling by LLL12 caused substantial increases in both OCR and ECAR in HCC1954 mock-transfected cells (Supp. Figs. 4*a*-4*d*), suggesting that IL-6 might decrease both parameters in these cells. On the contrary, only a modest increase in OCR was observed for HCC1954 NmU-overexpressing cells (Supp. Figs. 5*a*-5*d*). These results suggest that inhibition of IL-6 signalling increases cell metabolism, both respiratory and glycolytic, in control-transfected but not in NmU-overexpressing cells. However, since STAT3 is known to be involved in other signalling pathways, these results cannot solely be ascribed to IL-6 effects.

HER2-targeted drug-resistant cells also show altered cell bioenergetics

We have previously reported NmU to be expressed at higher levels in HER2-targeted drug-resistant cells compared to their drug sensitive counterparts, and we have also shown that overexpression of NmU conferred enhanced drug resistance and significantly increased migration and invasion traits on these cells [6]. We therefore speculated that the metabolic alterations observed in NmU-overexpressing cells might also occur in cells with acquired resistance to lapatinib, neratinib and trastuzumab (HCC1954 LR, HCC1954 NR, SKBR3 NR, and SKBR3 TR, respectively). As shown in Figure 4*a* and 3*c*, HCC1954 LR and HCC1954 NR cells showed significant decreases in OCR and all its associated parameters. Similar to the results obtained with NmU- and mock-transfected cells, the maximum OCR was not greater than the basal OCR, suggesting that these cells are already working at maximal activity in basal conditions. On the other hand, and similar to previous results with NmU-overexpressing variants, drug-resistant SKBR3 cells showed significant increases in basal and maximal OCR rates, with maximal OCR rates larger than basal values (Fig. 4*b* and *d*). Despite the decreased OCR in HCC1954 LR and HCC1954 NR cells when compared to parental cells, there appeared to be no significant increase in basal glycolytic flux (Fig. 5*a* and *c*); in fact, there was a decrease in ECAR which was more pronounced for HCC1954 NR cells. Similar to previous results, SKBR3 drug-resistant variants showed significant increases in glycolysis compared to parent, drug-sensitive cells (Fig. 5*b* and *d*). Once again, in spite of these differences, the OCR/ECAR ratios were significantly decreased for all drug-resistant variants compared to their drug-sensitive counterparts (Fig. 5*e* and *f*), particularly for HCC1954 cells. No clear correlation was found between bioenergetics profiles and proliferation rates (data not shown).

Similar to NmU-overexpressing cells, the decrease in OCR was not reflected in altered mitochondrial membrane potential (Supp. Fig. 2*b* and *c*). These results also demonstrate similar switches toward glycolysis in acquired drug-resistant cells compared to parental cells as those observed in NmU-overexpressing compared to mock-transfected cells.

NmU induces markers of EMT

A correlation between alterations in glucose metabolism and pathways involved in cell invasion and migration has been shown by others [9-12]. We previously reported that NmU-

overexpressing cells displayed increased migration and invasion abilities. These results are in agreement with the overall morphology of HCC1954 cell variants *i.e.* while HCC1954 Mock cells show a regular, almost polygonal shape, HCC1954 NmU cells are more spindle shaped with numerous protrusions (Fig. 6*a*), suggestive of a potentially more invasive phenotype. The increase in migration shown by NmU-overexpressing cells appears to be mediated through induction of epithelial to mesenchymal transition (EMT), a process typically characterised by loss of E-Cadherin and increased expression of vimentin and β-catenin, among other markers. As shown in Figure 6*b*, overexpression of NmU resulted in increased expression of β-catenin and also the soluble form of E-Cadherin (sE-Cadherin), which has been cleaved from the membrane and can no longer mediate cell-to-cell adhesion; although increased expression of vimentin in these cells was not statistically significant (results not shown). As expected, cells with acquired drug resistance also have increased expression of sE-Cadherin and vimentin (Fig. 6*c*). These results show that high expression levels of NmU are associated with EMT.

IL-6 secretion is increased by NmU

Previous studies have indicated that NmU is essential for the release of IL-6, a pro-inflammatory cytokine involved in numerous processes and implicated in malignancy and induction of EMT [13-15]. Interestingly, autocrine IL-6 signalling has been shown to promote migration, expansion of the cancer stem cell population and drug resistance in breast cancer cells, including trastuzumab resistance in HER2-positive cells [16-18]. As shown in Figures 7*a* and *b*, NmU-overexpressing HCC1954 NmU and SKBR3 NmU cells secrete significantly more IL-6 than their mock-transfected counterparts. Remarkably, even short-term (1 h) treatment of HCC1954 and SKBR3 cells with NmU peptide induced the release of IL-6 into the extracellular medium (Fig. 7*c* and *d*). As we thus hypothesised, the cells with acquired resistance to lapatinib and neratinib –which had previously been shown to express higher levels of NmU than their sensitive counterparts– also showed increased secretion of IL-6 (Fig. 7*e*). These results indicate that NmU is able to stimulate IL-6 secretion.

Moreover, extracellular IL-6 appears to play a role in the enhanced migration observed in HCC1954 NmU cells, since treatment with an antibody binding to the IL-6 receptor decreased the ability of these cells to migrate (Fig. 7*f*). Overall, our results suggest that NmU

mediates increased secretion of IL-6 in HER2-positive breast cancer cells; this appears to be one of the mechanisms through which NmU increases cell migration.

NmU overexpression induces expansion of the CSC population

Our results so far showed that NmU overexpression induced altered cell bioenergetics and EMT, and increased IL-6 secretion; all of these characteristics have been associated with the CSC phenotype. It was therefore evident that we should investigate the CSC phenotype in NmU-overexpressing cells. As shown in Figures 8*a* and *b*, HCC1954 NmU and SKBR3 NmU cells showed significantly increased populations of $CD44^+/CD24^-$ cells, compared to HCC1954 Mock and SKBR3 Mock cells, as determined by flow cytometry. Supporting these results, NmU-overexpressing cells also showed increased expression of aldehyde dehydrogenase 1 (ALDH1), an enzyme also associated with the CSC phenotype (Fig. 8*c* and Supplementary Figure 6). As expected based on this, the acquired drug-resistant cells also displayed an expanded $CD44^+/CD24^-$ population (Fig. 8*d*). Overall, these results suggest that the alterations mediated by NmU overexpression causes expansion of cells with CSC phenotype in HER2-positive breast cancer cells.

To further confirm the link between NmU and the CSC phenotype, $CD44^+/CD24^-$ cells were subsequently separated by flow cytometry cell sorting from the whole HCC1954 cell population, and compared to cells with non-CSC phenotype. In agreement with previous findings [18], we found the breast tumour cells with CSC phenotype to secrete increased amounts of IL-6 (Fig. 8*e*) and TGFβ (Fig. 8*f*). Interestingly, cells with CSC phenotype also displayed increased levels of NmU, both in cell lysates and in conditioned medium (Fig. 8*g* and *h*). These results confirm the association between high levels of NmU and the CSC phenotype.

Discussion

In this study we have identified NmU as a master regulator of traits associated with the CSC phenotype, including altered metabolism, EMT features and increased IL-6 secretion. Overexpression of NmU thus results in expansion of the CSC population in HER2-positive breast cancer cells.

Our results showed that NmU-overexpressing cells have switched from preferential use of mitochondrial respiration to glycolysis, as determined by their OCR/ECAR rates. Similar results were observed in cells with acquired resistance to lapatinib, neratinib and trastuzumab, which express significantly increased amounts of NmU compared to their drug-sensitive parent counterparts. Interestingly, short-term treatment with exogenous NmU was sufficient to cause a significant increase in ECAR, suggesting that increased levels of NmU in the extracellular medium are enough to cause metabolic alterations.

Although altered, both metabolic pathways –mitochondrial respiration and glycolysis– were functional in all the cell lines tested, as shown by changes in OCR and ECAR following treatment with the ATP synthase inhibitor oligomycin. The results show that metabolic alterations vary in different cell lines, with SKBR3 cells increasing their respiration when overexpressing NmU or acquiring resistance to HER2-targeted drugs. This is in contrast to what we observed in drug-resistant HCC1954 cells, which either obtain their energy from an alternative source (*i.e.* not respiration nor glycolysis), or have adapted their metabolism to reduce their energetic requirements to a minimum. The decrease in oxygen consumption rules out oxidative metabolic pathways such as lipid oxidation, suggesting that the latter scenario is most likely. However, further experiments would be needed to fully elucidate these phenomena.

The results obtained in the more aggressive cell variants (i.e. NmU-overexpressing drug-resistant) were not apparently due to altered mitochondrial potential, suggesting that mitochondria are not dysfunctional in these cells. The reason for the observed switch to glycolysis caused by NmU overexpression appears to be enhanced pyruvate dehydrogenase kinase activity, as treatment with an inhibitor of this enzyme caused a significant increase in the OCR in NmU-overexpressing HCC1954 cells but not in control cells.

Finally, we decided to evaluate the role of IL-6 in the observed metabolic alterations. Consistent with it having a role as a downstream effector of NmU, IL-6 has also been involved in processes related to energy, feeding and metabolism, as it is produced by adipose tissue and its levels are regulated by hormones that modulate metabolism [8. 19]. A previous study reported a role for IL-6 in increased glucose uptake and insulin resistance [20]. However, to the best of our knowledge, all such studies have been performed *in vivo* in

laboratory animals or patients, and the effects of IL-6 signalling at the cellular level remain unclear. Treatment of NmU-overexpressing cells with an inhibitor of STAT3 -a key downstream mediator of IL-6 signalling- caused only a modest increase in OCR in NmU-overexpressing cells, while it caused dramatic increases in both OCR and ECAR in mock-transfected cells. These results suggest that IL-6 signalling may be reducing both mitochondrial respiration and glycolysis in drug-sensitive, less migratory parent cells. This role appears to be decreased in NmU-overexpressing cells, suggesting an altered role of IL-6 in metabolic regulation and possibly development of IL-6 resistance. However, it should be noted that STAT3 inhibition can affect signalling through many different pathways, including that of HER2, and as such the specific role of IL-6 in these cells needs to be confirmed by further experiments.

Previous reports have shown that altered glucose metabolism is associated with CSCs and may even be considered a hallmark of the CSC phenotype [reviewed in [3]]. This is because CSCs -being self-renewing and also having the ability to differentiate into multiple cell lineages- require large amounts of cellular macromolecules and thus cannot afford for the majority of glucose to be used for ATP production by mitochondrial oxidation. It has been proposed by others that, although the CSC phenotype is dynamic and shows a plasticity dependent on environmental cues, aberrant metabolism is a prerequisite of stemness, without which the CSC phenotype cannot develop [3, 21]. Based on our study, it is reasonable to propose that increased levels of NmU are inducing this aberrant metabolism and facilitating the establishment of the CSC phenotype.

EMT is a transformation process usually linked to increased migration and invasion abilities, but it has also been associated with drug resistance [22-24] and the CSC phenotype [25-26]. For example, non-small cell lung cancer cells resistant to erlotinib (an EGFR/HER1-targeting drug) displayed EMT features [27]. Links have also been reported between pyruvate dehydrogenase kinase activity and EMT in colon cancer cells, where levels of this enzyme were correlated with EMT features and resistance to conventional chemotherapeutic drugs [28-31]. In keeping with these results, NmU-overexpressing cells also displayed increased expression of EMT markers as well as enhanced pyruvate dehydrogenase kinase activity. Interestingly, IL-6 has been reported to be an EMT inducer in breast cancer cells [32-33].

NmU has been proposed to modulate cytokine release; indeed, macrophages from mice deficient in NmU are unable to release IL-6 in response to pro-inflammatory challenges [13-15]. Our results show that increased expression of NmU –whether ectopically overexpressed or acquired by cells after prolonged exposure to HER2-targeting drugs– results in increased amounts of secreted IL-6. Even short-term treatment of cells with NmU was able to elicit release of pre-formed IL-6 (judging by the timing of the effect). IL-6 has been shown to induce the CSC phenotype in some cancer types, including breast cancer [18, 34-35] and here NmU-overexpressing cells –as well as HER2-targeted drug-resistant cells– were shown to have an increased proportion of CSC cells. CSCs are notoriously resistant to chemotherapy and radiotherapy and an increased proportion of these cells has been proposed to be the reason behind the increased resistance to trastuzumab in cancer cells [18]. Therefore, our observation of an expansion of cells with CSC phenotype mediated by NmU could explain the increase in drug resistance associated with NmU-overexpression. Our previous results had shown that NmU partners with Hsp27 [6]. The relevance of the NmU:Hsp27 partnering to the study described here is supported by the fact that Hsp27 is increased in the CSC sub-population of AS-B145 and AS-B244 breast cells, with subsequent Hsp27 knock-down suppressing EMT and decreased CSC frequency *in vitro* and *in vivo* [36]. Furthermore, in prostate cancer Hsp27 is reported as a critical regulator in IL-6-dependent and IL-6-independent EMT [37]. The identification of NmU as a partner of Hsp27 is a novel observation that may be contributing to this chain of events, with NmU being an autocrine/paracrine factor that alters the dynamic equilibrium of cells with CSC phenotype within the overall cancer cell population. Supporting this notion, it has recently been reported that knock-down of NmU expression in endometrial cancer cells reduces the mRNA transcript levels of the CSC marker CD44 [38].

In conclusion, NmU is an attractive target for HER2-overexpressing breast cancer, but the multiple physiological roles it has been proposed to play may make it challenging to alter its function without side-effects. The identification of downstream effects of NmU signaling, such as increased IL-6 levels and increased glycolysis, suggest novel ways in which NmU function can be targeted for the treatment of HER2-overexpressing breast cancer and controlling the otherwise increased proportion of cells with CSC phenotype. Combination

with therapies that block these downstream effectors of NmU could then add value to currently approved HER2-targeted therapies.

Acknowledgements

The authors wish to acknowledge funding from HRB's Health Research Award [HRA-POR-2014-658]; Irish Cancer Society's Breast-Predict [CCRC13GAL]; Trinity Foundation, Development and Alumni and HEA's PRTLI Cycle 5 support of TBSI.

References

1. Ferreira LM. Cancer metabolism: the Warburg effect today. Exp Mol Pathol 2010; 89: 372-380

2. Zhao Y, Butler EB, Tan M. Targeting cellular metabolism to improve cancer therapeutics. Cell Death Dis 2013; 4: e532

3. Menendez JA, Joven J, Cufi S, Corominas-Faja B, Oliveras-Ferraros C, Cuyas E, Martin-Castillo B, Lopez-Bonet E, Alarcon T, Vazquez-Martin A. The Warburg effect version 2.0: metabolic reprogramming of cancer stem cells. Cell Cycle 2013; 12: 1166-1179

4. Mitchell JD, Maguire JJ, Davenport AP. Emerging pharmacology and physiology of neuromedin U and the structurally related peptide neuromedin S. Br J Pharmacol 2009; 158: 87-103

5. Martinez VG, O'Driscoll L. Neuromedin U: a multifunctional neuropeptide with pleiotropic roles. Clin Chem 2015; 61: 471-482

6. Rani S, Corcoran C, Shiels L, Germano S, Breslin S, Madden S, McDermott MS, Browne BC, O'Donovan N, Crown J, Gogarty M, Byrne AT, et al. Neuromedin U: A Candidate Biomarker and Therapeutic Target to Predict and Overcome Resistance to HER-Tyrosine Kinase Inhibitors. Cancer Res 2014; 74: 3821-3833

7. Jacobson J, Duchen MR, Heales SJ. Intracellular distribution of the fluorescent dye nonyl acridine orange responds to the mitochondrial membrane potential: implications for assays of cardiolipin and mitochondrial mass. J Neurochem 2002; 82: 224-233

8. Mauer J, Denson JL, Bruning JC. Versatile functions for IL-6 in metabolism and cancer. Trends Immunol 2015; 36: 92-101

9. Vander Heiden MG, Locasale JW, Swanson KD, Sharfi H, Heffron GJ, Amador-Noguez D, Christofk HR, Wagner G, Rabinowitz JD, Asara JM, Cantley LC. Evidence for an alternative glycolytic pathway in rapidly proliferating cells. Science 2010; 329: 1492-1499

10. Locasale JW, Cantley LC. Metabolic flux and the regulation of mammalian cell growth. Cell Metab 2011; 14: 443-451

11. Graham NA, Tahmasian M, Kohli B, Komisopoulou E, Zhu M, Vivanco I, Teitell MA, Wu H, Ribas A, Lo RS, Mellinghoff IK, Mischel PS, et al. Glucose deprivation activates a metabolic and signaling amplification loop leading to cell death. Mol Syst Biol 2012; 8: 589

12. Komurov K, Tseng JT, Muller M, Seviour EG, Moss TJ, Yang L, Nagrath D, Ram PT. The glucose-deprivation network counteracts lapatinib-induced toxicity in resistant ErbB2-positive breast cancer cells. Mol Syst Biol 2012; 8: 596

13. Johnson EN, Appelbaum ER, Carpenter DC, Cox RF, Disa J, Foley JJ, Ghosh SK, Naselsky DP, Pullen MA, Sarau HM, Scheff SR, Steplewski KM, et al. Neuromedin U elicits cytokine release in murine Th2-type T cell clone D10.G4.1. J Immunol 2004; 173: 7230-7238

14. Moriyama M, Matsukawa A, Kudoh S, Takahashi T, Sato T, Kano T, Yoshimura A, Kojima M. The neuropeptide neuromedin U promotes IL-6 production from macrophages and endotoxin shock. Biochem Biophys Res Commun 2006; 341: 1149-1154

15. Abbondanzo SJ, Manfra DJ, Chen SC, Pinzon-Ortiz M, Sun Y, Phillips JE, Laverty M, Vassileva G, Hu W, Yang S, Gustafson EL, Fine JS, et al. Nmur1-/- mice are not protected from cutaneous inflammation. Biochem Biophys Res Commun 2009; 378: 777-782

16. Badache A, Hynes NE. Interleukin 6 inhibits proliferation and, in cooperation with an epidermal growth factor receptor autocrine loop, increases migration of T47D breast cancer cells. Cancer Res 2001; 61: 383-391

17. Conze D, Weiss L, Regen PS, Bhushan A, Weaver D, Johnson P, Rincon M. Autocrine production of interleukin 6 causes multidrug resistance in breast cancer cells. Cancer Res 2001; 61: 8851-8858

18. Korkaya H, Kim GI, Davis A, Malik F, Henry NL, Ithimakin S, Quraishi AA, Tawakkol N, D'Angelo R, Paulson AK, Chung S, Luther T, et al. Activation of an IL6 inflammatory loop mediates trastuzumab resistance in HER2+ breast cancer by expanding the cancer stem cell population. Mol Cell 2012; 47: 570-584

19. Papanicolaou DA, Vgontzas AN. Interleukin-6: the endocrine cytokine. J Clin Endocrinol Metab 2000; 85: 1331-1333

20. Carey AL, Steinberg GR, Macaulay SL, Thomas WG, Holmes AG, Ramm G, Prelovsek O, Hohnen-Behrens C, Watt MJ, James DE, Kemp BE, Pedersen BK, et al. Interleukin-6 increases insulin-stimulated glucose disposal in humans and glucose uptake and fatty acid oxidation in vitro via AMP-activated protein kinase. Diabetes 2006; 55: 2688-2697

21. Folmes CD, Nelson TJ, Dzeja PP, Terzic A. Energy metabolism plasticity enables stemness programs. Ann N Y Acad Sci 2012; 1254: 82-89

22. Yauch RL, Januario T, Eberhard DA, Cavet G, Zhu W, Fu L, Pham TQ, Soriano R, Stinson J, Seshagiri S, Modrusan Z, Lin CY, et al. Epithelial versus mesenchymal phenotype determines in vitro sensitivity and predicts clinical activity of erlotinib in lung cancer patients. Clin Cancer Res 2005; 11: 8686-8698

23. Creighton CJ, Li X, Landis M, Dixon JM, Neumeister VM, Sjolund A, Rimm DL, Wong H, Rodriguez A, Herschkowitz JI, Fan C, Zhang X, et al. Residual breast cancers after conventional

therapy display mesenchymal as well as tumor-initiating features. Proc Natl Acad Sci U S A 2009; 106: 13820-13825

24. Thiery JP, Acloque H, Huang RY, Nieto MA. Epithelial-mesenchymal transitions in development and disease. Cell 2009; 139: 871-890

25. Chaffer CL, Marjanovic ND, Lee T, Bell G, Kleer CG, Reinhardt F, D'Alessio AC, Young RA, Weinberg RA. Poised chromatin at the ZEB1 promoter enables breast cancer cell plasticity and enhances tumorigenicity. Cell 2013; 154: 61-74

26. Mani SA, Guo W, Liao MJ, Eaton EN, Ayyanan A, Zhou AY, Brooks M, Reinhard F, Zhang CC, Shipitsin M, Campbell LL, Polyak K, et al. The epithelial-mesenchymal transition generates cells with properties of stem cells. Cell 2008; 133: 704-715

27. Yao Z, Fenoglio S, Gao DC, Camiolo M, Stiles B, Lindsted T, Schlederer M, Johns C, Altorki N, Mittal V, Kenner L, Sordella R. TGF-beta IL-6 axis mediates selective and adaptive mechanisms of resistance to molecular targeted therapy in lung cancer. Proc Natl Acad Sci U S A 2010; 107: 15535-15540

28. Lu CW, Lin SC, Chen KF, Lai YY, Tsai SJ. Induction of pyruvate dehydrogenase kinase-3 by hypoxia-inducible factor-1 promotes metabolic switch and drug resistance. J Biol Chem 2008; 283: 28106-28114

29. Lu CW, Lin SC, Chien CW, Lee CT, Lin BW, Lee JC, Tsai SJ. Overexpression of pyruvate dehydrogenase kinase 3 increases drug resistance and early recurrence in colon cancer. Am J Pathol 2011; 179: 1405-1414

30. Sun Y, Daemen A, Hatzivassiliou G, Arnott D, Wilson C, Zhuang G, Gao M, Liu P, Boudreau A, Johnson L, Settleman J. Metabolic and transcriptional profiling reveals pyruvate dehydrogenase kinase 4 as a mediator of epithelial-mesenchymal transition and drug resistance in tumor cells. Cancer Metab 2014; 2: 20

31. Zhang Y, Geng L, Yi H, Huo W, Talmon G, Kim YC, Wang SM, Wang J. Transforming Growth Factor beta Mediates Drug Resistance by Regulating the Expression of Pyruvate Dehydrogenase Kinase 4 in Colorectal Cancer. J Biol Chem 2016; 291: 17405-17416

32. Sullivan NJ, Sasser AK, Axel AE, Vesuna F, Raman V, Ramirez N, Oberyszyn TM, Hall BM. Interleukin-6 induces an epithelial-mesenchymal transition phenotype in human breast cancer cells. Oncogene 2009; 28: 2940-2947

33. Xie G, Yao Q, Liu Y, Du S, Liu A, Guo Z, Sun A, Ruan J, Chen L, Ye C, Yuan Y. IL-6-induced epithelial-mesenchymal transition promotes the generation of breast cancer stem-like cells analogous to mammosphere cultures. Int J Oncol 2012; 40: 1171-1179

34. Iliopoulos D, Hirsch HA, Struhl K. An epigenetic switch involving NF-kappaB, Lin28, Let-7 MicroRNA, and IL6 links inflammation to cell transformation. Cell 2009; 139: 693-706

35. Iliopoulos D, Hirsch HA, Wang G, Struhl K. Inducible formation of breast cancer stem cells and their dynamic equilibrium with non-stem cancer cells via IL6 secretion. Proc Natl Acad Sci U S A 2011; 108: 1397-1402

36. Wei L, Liu TT, Wang HH, Hong HM, Yu AL, Feng HP, Chang WW. Hsp27 participates in the maintenance of breast cancer stem cells through regulation of epithelial-mesenchymal transition and nuclear factor-kappaB. Breast Cancer Res 2011; 13: R101

37. Shiota M, Bishop JL, Nip KM, Zardan A, Takeuchi A, Cordonnier T, Beraldi E, Bazov J, Fazli L, Chi K, Gleave M, Zoubeidi A. Hsp27 regulates epithelial mesenchymal transition, metastasis, and circulating tumor cells in prostate cancer. Cancer Res 2013; 73: 3109-3119

38. Lin TY, Wu FJ, Chang CL, Li Z, Luo CW. NMU signaling promotes endometrial cancer cell progression by modulating adhesion signaling. Oncotarget 2016; 7: 10228-10242

Figure legends

Fig. 1. NmU-overexpressing cells show altered OCR. *a* and *b*, OCR was measured by Seahorse XF24 in HCC1954 (*a*) and SKBR3 (*b*) cell variants following the sequential addition of oligomycin A, FCCP and rotenone/antimycin A. *c* and *d*, metabolic parameters calculated from the OCR. ATP-linked OCR was determined by subtracting the proton leak measure from the basal OCR measure. Reserve capacity was determined by subtracting the basal OCR measure from the maximum OCR measure. Data are expressed as the mean ± SEM of 3 independent experiments. *p≤0.05, **p≤0.01, ***p≤ 0.001.

Fig. 2. NmU-overexpressing cells show altered ECAR. *a* and *b*, ECAR was measured by Seahorse XF24 in HCC1954 (*a*) and SKBR3 (*b*) cell variants following the sequential addition of oligomycin A, FCCP and rotenone/antimycin A. *c* and *d*, metabolic parameters calculated from the ECAR. Glycolytic reserve was determined by subtracting the basal ECAR measure from the maximum ECAR measure. *e* and *f*, Ratios were obtained by dividing the basal and maximal OCR by their corresponding ECAR. Data are expressed as the mean ± SEM of 3 independent experiments. *p≤0.05, **p≤0.01, ***p≤ 0.001.

Fig. 3. Inhibition of pyruvate dehydrogenase kinase by DCA increases oxygen consumption in NmU-overexpressing cells. HCC1954 cells were treated with 5mM DCA for 72 h before Seahorse analysis. *a* and *c*, OCR was measured in HCC1954 Mock and HCC1954 NmU cells, respectively, using the Seahorse XF24 following the sequential addition of oligomycin A, FCCP and rotenone/antimycin A. *b* and *d*, ECAR was measured in HCC1954 Mock and HCC1954 NmU cells, respectively, by Seahorse following the sequential addition of oligomycin A, FCCP and rotenone/antimycin A. Metabolic parameters were calculated from the OCR and ECAR data. ATP-linked OCR was determined by subtracting the proton leak measure from the basal OCR measure. Reserve capacity was determined by subtracting the basal OCR measure from the maximum OCR measure. Glycolytic reserve was determined by subtracting the basal ECAR measure from the maximum ECAR measure. Data are expressed as the mean ± SEM of 3 independent experiments. *p≤0.05, **p≤0.01, ***p≤ 0.001.

Fig. 4. Cells with acquired resistance to HER2-targeted drugs show altered OCR. *a* and *b*, OCR was measured by Seahorse XF24 in HCC1954 (*a*) and SKBR3 (*b*) drug-resistant cell variants following the sequential addition of oligomycin A, FCCP and rotenone/antimycin A. *c* and *d*, metabolic parameters calculated from the OCR. ATP-linked OCR was determined by subtracting the proton leak measure from the basal OCR measure. Reserve capacity was determined by subtracting the basal OCR measure from the maximum OCR measure. Data are expressed as the mean ± SEM of 3 independent experiments. *p≤0.05, **p≤0.01, ***p≤ 0.001.

Fig. 5. Cells with acquired resistance to HER2-targeted drugs show altered ECAR. *a* and *b*, ECAR was measured by Seahorse XF24 in HCC1954 (*a*) and SKBR3 (*b*) drug-resistant cell variants following the sequential addition of oligomycin A, FCCP and rotenone/antimycin A. *c* and *d*, metabolic parameters calculated from the ECAR. Glycolytic reserve was determined by subtracting the basal ECAR measure from the maximum ECAR measure. *e* and *f*, Ratios were obtained by dividing the basal and maximal OCR by their corresponding ECAR. Data are expressed as the mean ± SEM of 3 independent experiments. *p≤0.05, **p≤0.01, ***p≤ 0.001.

Fig. 6. NmU overexpression correlates with induction of EMT markers. *a*, Morphology of HCC1954 Mock and HCC1954 NmU cells by light microscopy. *b*, Total cell lysates were

obtained from HCC1954 Mock and NmU cells. sE-Cadherin, β-catenin and vimentin were detected by immunoblotting. β-actin was used as loading control. Densitometry was performed on bands using QuantityOne software. *c*, Same as in *b* with HCC1954 Par, HCC1954 LR and HCC1954 NR cells. Results represent the average of at least three independent experiments. *p≤0.05, **p≤0.01, ***p≤ 0.001.

Fig. 7. NmU overexpression correlates with increased IL-6 secretion. *a*, *b* and *e*, IL-6 levels were determined by ELISA in serum-free cell supernatants of HCC1954 and SKBR3 cell variants and expressed as ng IL-6 per mg total cell protein. *c* and *d*, HCC1954 and SKBR3 cells were seeded at $1x10^5$ in a 24-well plate, serum starved overnight and incubated with NmU peptide for 60 min at 37°C. IL-6 levels were determined by ELISA in serum-free cell supernatant and expressed as ng IL-6 per mg total cell protein. *f(i)*, Cell motility was assessed by the wound healing assay in the presence or absence of the monoclonal antibody Tocilizumab (aIL-6R). *f(ii)*, percent of closure relative to wound at time=0 was evaluated after 24 h. Results represent the average of at least three independent experiments. *p<0.05, **p<0.01, ***p< 0.001.

Fig. 8. NmU overexpression correlates with expansion of cells with cancer stem cell phenotype. *a* and *b*, HCC1954 and SKBR3 cells, respectively, were stained with anti-CD24 and anti-CD44 and followed by FACS analysis in a FACSCanto II flow cytometer. Results are expressed as fold difference relative to control transfected cells. *c*, Expression of ALDH1 was evaluated by immunoblotting in cell lysates in triplicate, with expression of β-actin used as control. Densitometry was performed using QuantityOne software. *d*, HCC1954 cell variants were stained with anti-CD24 and anti-CD44, followed by FACS analysis in a FACSCanto II flow cytometer. *e*, HCC1954 cells were stained with anti-CD44 and anti-CD24 and separated by sorting in a FACSAria flow cytometer into $CD44^+/CD24^-$ (CSC phenotype) and non-CSC phenotype. IL-6 levels were then determined in conditioned medium as before. *f*, Same as before but $TGF\beta_1$ levels were determined by ELISA. *g*, Same as before, but NmU levels were determined in cell lysates by ELISA. *h*, Same as in *g*, but NmU levels were determined in conditioned medium. Results represent the average of at least three independent experiments. *p<0.05, **p<0.01, ***p<0.001.

Supplementary Figure 1. Schematic representations of Seahorse XF24 data. *a*, The basal oxygen consumption rate (OCR) is measured by a Seahorse XF24 instrument and changes to it are recorded following sequential injections of oligomycin, FCCP, rotenone and antimycin. The proton leak refers to the contribution of non-ATP–linked oxygen consumption (following oligomycin injection), while ATP–linked respiration can be calculated from subtracting the proton leak from the basal respiration values. The maximal respiration capacity was determined using the FCCP-stimulated rate. The reserve capacity was represented by the maximal OCR subtracted from the baseline OCR. The residual oxygen consumption that occurred after addition of rotenone and antimycin A was ascribed to non-mitochondrial respiration. *b*, The basal extracellular acidification rate (ECAR) is measured by a Seahorse XF24 instrument and changes to it are recorded following sequential injections of oligomycin and 2-DG. The maximal ECAR rate was determined using the oligomycin-stimulated rate, while the glycolytic reserve was calculated by subtracting the basal ECAR from the maximal ECAR. Residual extracellular acidification following addition of 2-deoxyglucose was ascribed to non-glycolytic acidification.

Supplementary Figure 2. Cells were stained with 10μM NAO for 10 min, washed and analysed by FACS. *a*, HCC1954 Mock (red) and HCC1954 NmU (grey) cells. *b*, HCC1954 Par (red) and HCC1954 LR (grey) cells. *c*, HCC1954 Par (red) and HCC1954 NR (grey) cells.

Supplementary Figure 3. Short-term treatment with NmU induces changes in cell bioenergetics. Cells were treated with 1μM NmU for 72 h before Seahorse analysis. *a(i)*, OCR was measured in the Seahorse XF24 instrument following the sequential addition of oligomycin A and FCCP. *a(ii)*, metabolic parameters calculated from the OCR. *b(i)*, ECAR was measured in the Seahorse XF24 instrument following the sequential addition of oligomycin A and FCCP. *b(ii)*, metabolic parameters calculated from the ECAR. *c*, Ratios were obtained by dividing the basal and maximal OCR by their corresponding ECAR. Data are expressed as the mean ± SEM of 3 independent experiments. *p≤0.05, **p≤0.01, ***p≤ 0.001.

Supplementary Figure 4. HCC1954 Mock cells were treated with 0.1μM LLL12 for 72 h before Seahorse analysis. *a,* OCR was measured by Seahorse XF24 following the sequential addition of oligomycin A, FCCP and rotenone/antimycin A. *b,* ECAR was measured by Seahorse following the sequential addition of oligomycin A, FCCP and rotenone/antimycin A.

c, Metabolic parameters were calculated from the OCR. ATP-linked OCR was determined by subtracting the proton leak measure from the basal OCR measure. Reserve capacity was determined by subtracting the basal OCR measure from the maximum OCR measure. *d,* Metabolic parameters were calculated from the ECAR. Glycolytic reserve was determined by subtracting the basal ECAR measure from the maximum ECAR measure. Data are expressed as the mean ± SEM of 3 independent experiments. *p≤0.05, **p≤0.01, ***p≤ 0.001.

Supplementary Figure 5. HCC1954 NmU cells were treated with 0.1μM LLL12 for 72 h before Seahorse analysis. *a,* OCR was measured by Seahorse XF24 following the sequential addition of oligomycin A, FCCP and rotenone/antimycin A. *b,* ECAR was measured by Seahorse following the sequential addition of oligomycin A, FCCP and rotenone/antimycin A. *c,* Metabolic parameters were calculated from the OCR. ATP-linked OCR was determined by subtracting the proton leak measure from the basal OCR measure. Reserve capacity was determined by subtracting the basal OCR measure from the maximum OCR measure. *d,* Metabolic parameters were calculated from the ECAR. Glycolytic reserve was determined by subtracting the basal ECAR measure from the maximum ECAR measure. Data are expressed as the mean ± SEM of 3 independent experiments. *p≤0.05, **p≤0.01, ***p≤ 0.001.

Supplementary Figure 6. Cell lysates (30μg) were separated by SDS-PAGE and probed with an anti-ALDH1 antibody. Molecular weight of ALDH1 is 53-55 kDa. β-actin was evaluated as control.

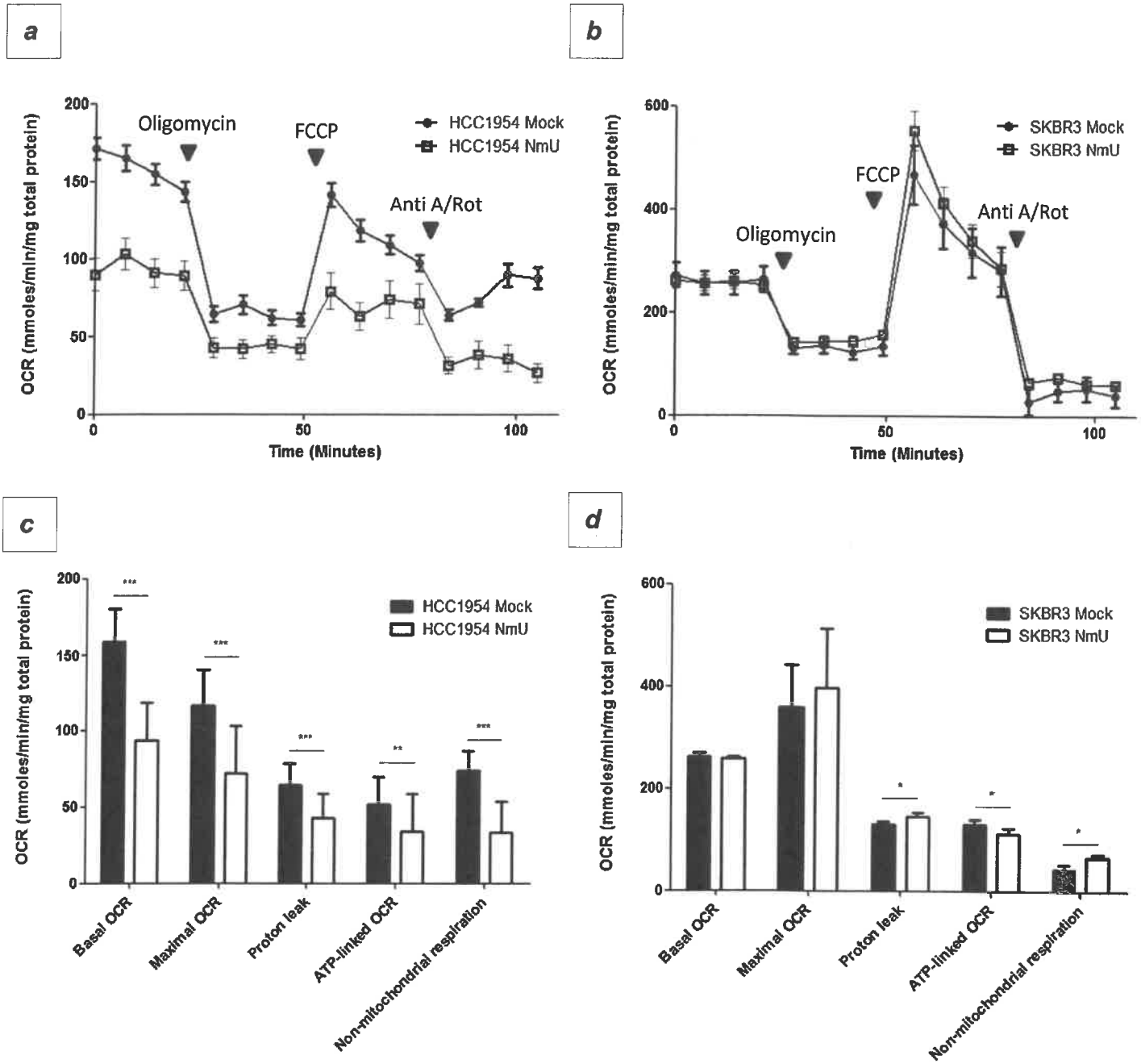
a
b
c
d
OCR (mmoles/min/mg total protein)
Time (Minutes)
Oligomycin
FCCP
Anti A/Rot
HCC1954 Mock
HCC1954 NmU
SKBR3 Mock
SKBR3 NmU
Basal OCR
Maximal OCR
Proton leak
ATP-linked OCR
Non-mitochondrial respiration

Figure 1

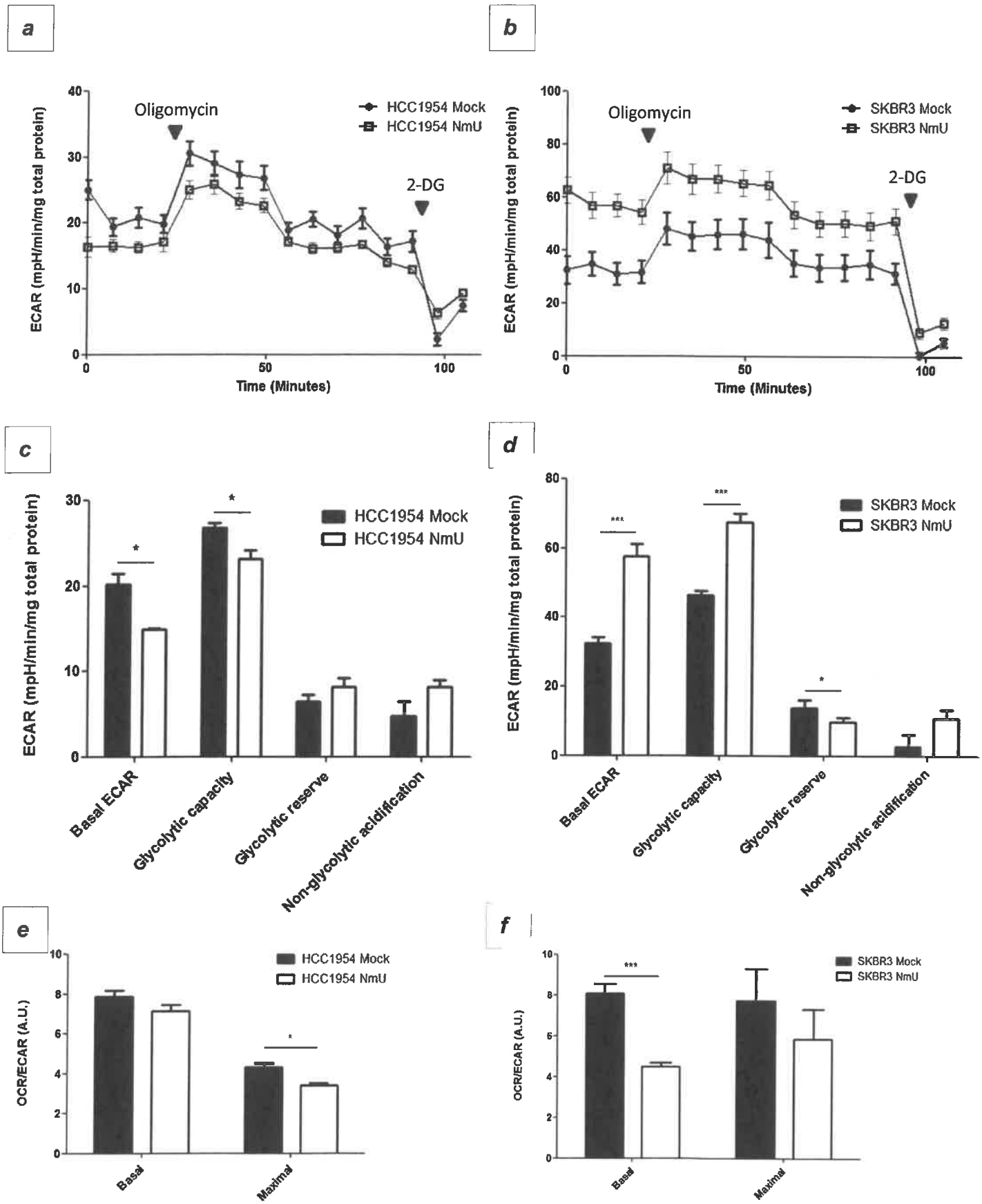
a
b
Oligomycin
2-DG
HCC1954 Mock
HCC1954 NmU
SKBR3 Mock
SKBR3 NmU
ECAR (mpH/min/mg total protein)
Time (Minutes)
c
d
Basal ECAR
Glycolytic capacity
Glycolytic reserve
Non-glycolytic acidification
e
f
OCR/ECAR (A.U.)
Basal
Maximal

Figure 2

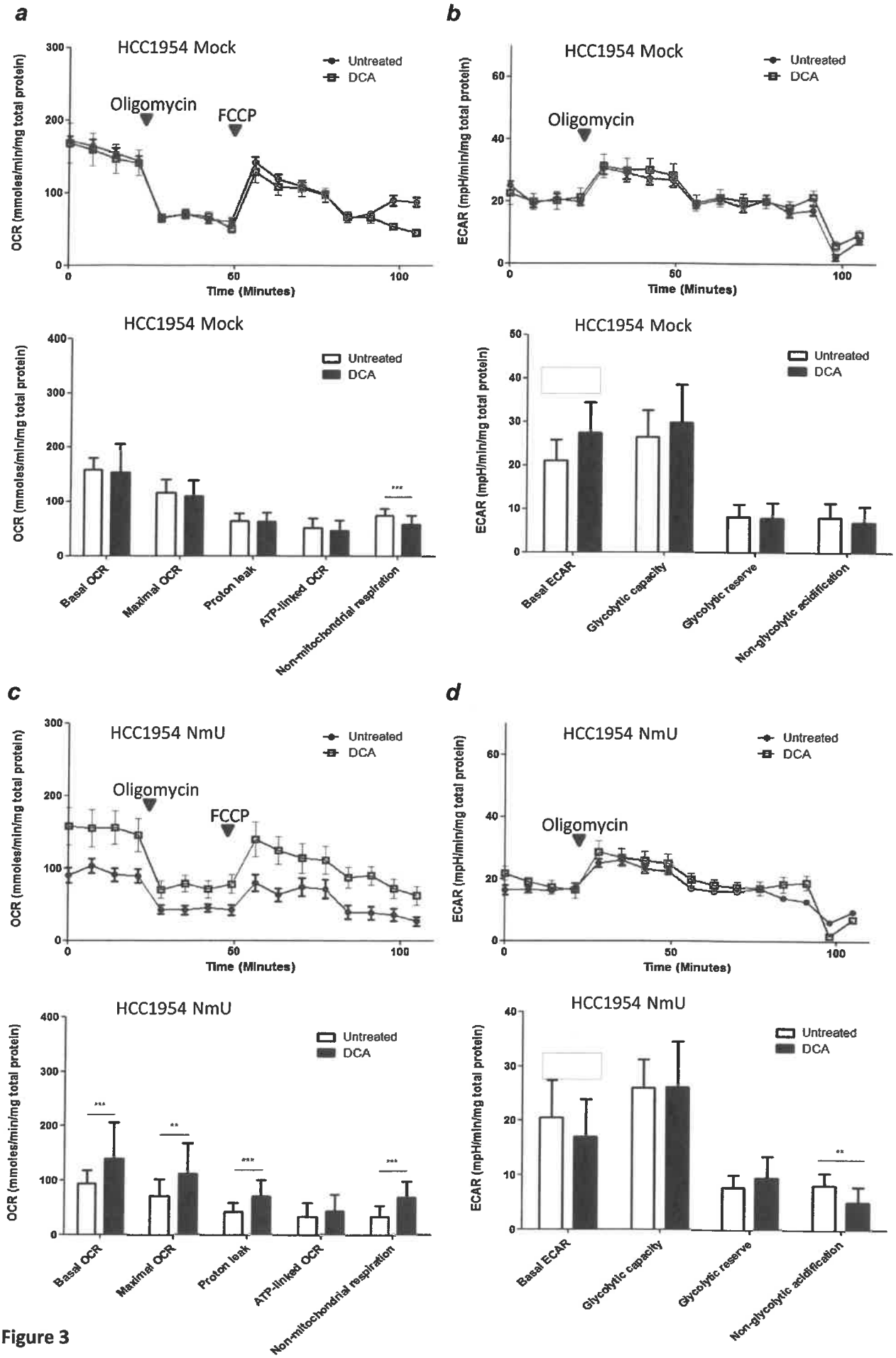
a
HCC1954 Mock
Untreated
DCA
Oligomycin
FCCP
OCR (mmoles/min/mg total protein)
Time (Minutes)
HCC1954 Mock
Untreated
DCA
OCR (mmoles/min/mg total protein)
Basal OCR
Maximal OCR
Proton leak
ATP-linked OCR
Non-mitochondrial respiration
b
HCC1954 Mock
Untreated
DCA
Oligomycin
ECAR (mpH/min/mg total protein)
Time (Minutes)
HCC1954 Mock
Untreated
DCA
ECAR (mpH/min/mg total protein)
Basal ECAR
Glycolytic capacity
Glycolytic reserve
Non-glycolytic acidification
c
HCC1954 NmU
Untreated
DCA
Oligomycin
FCCP
OCR (mmoles/min/mg total protein)
Time (Minutes)
HCC1954 NmU
Untreated
DCA
OCR (mmoles/min/mg total protein)
Basal OCR
Maximal OCR
Proton leak
ATP-linked OCR
Non-mitochondrial respiration
d
HCC1954 NmU
Untreated
DCA
Oligomycin
ECAR (mpH/min/mg total protein)
Time (Minutes)
HCC1954 NmU
Untreated
DCA
ECAR (mpH/min/mg total protein)
Basal ECAR
Glycolytic capacity
Glycolytic reserve
Non-glycolytic acidification

Figure 3

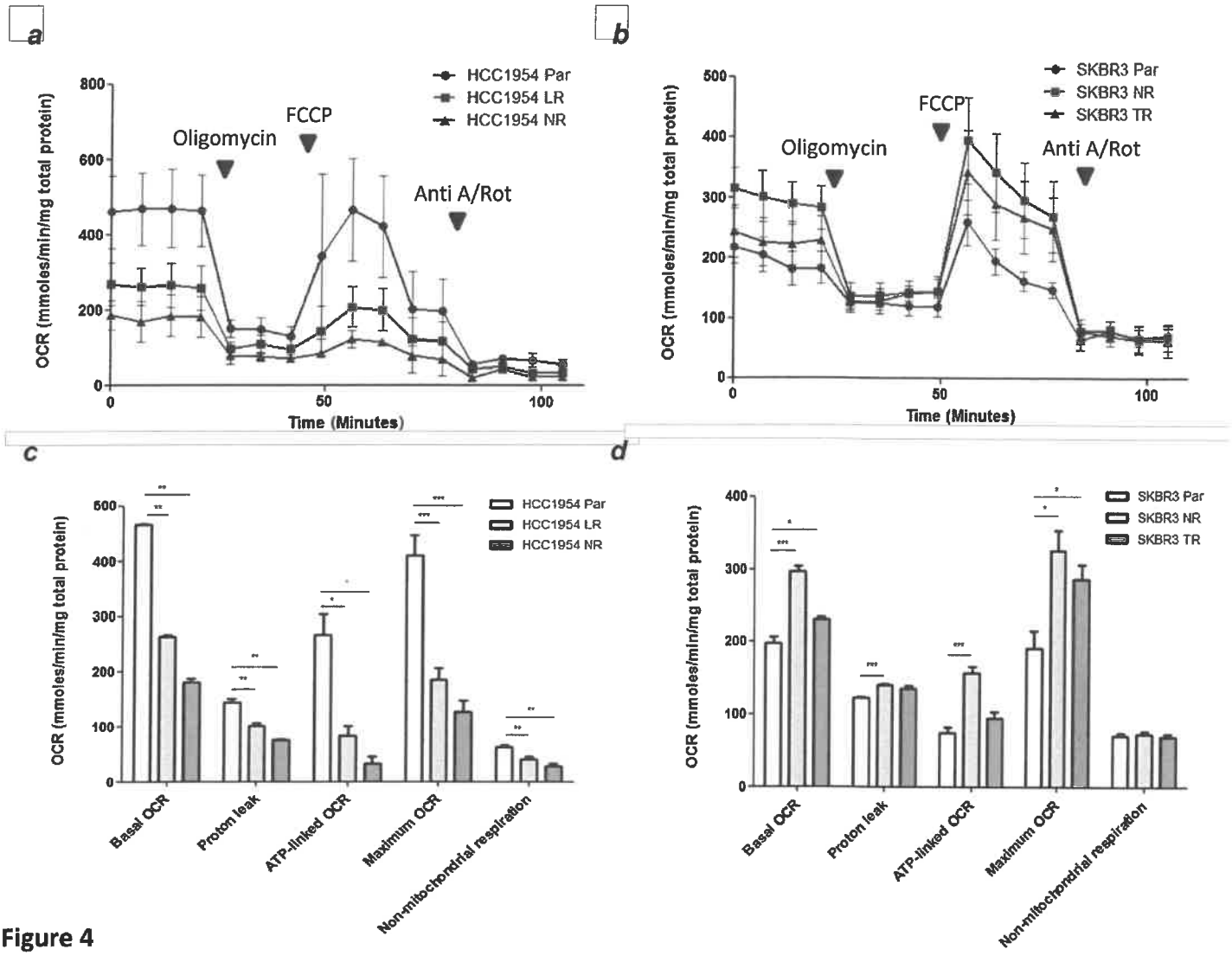
a
b
c
d
OCR (mmoles/min/mg total protein)
Time (Minutes)
Oligomycin
FCCP
Anti A/Rot
HCC1954 Par
HCC1954 LR
HCC1954 NR
SKBR3 Par
SKBR3 NR
SKBR3 TR
Basal OCR
Proton leak
ATP-linked OCR
Maximum OCR
Non-mitochondrial respiration

Figure 4

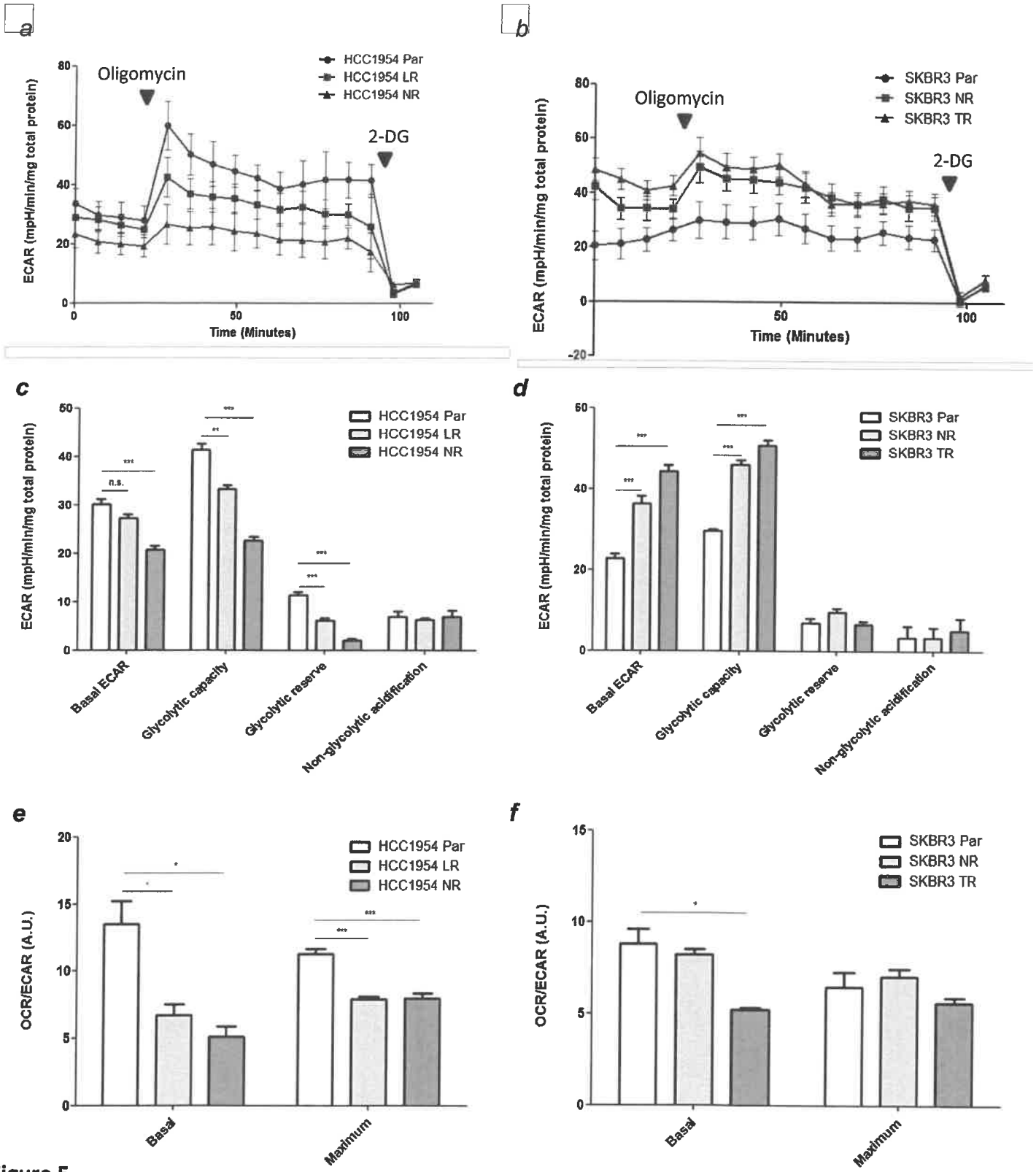
a
Oligomycin
2-DG
HCC1954 Par
HCC1954 LR
HCC1954 NR
ECAR (mpH/min/mg total protein)
Time (Minutes)
b
Oligomycin
2-DG
SKBR3 Par
SKBR3 NR
SKBR3 TR
ECAR (mpH/min/mg total protein)
Time (Minutes)
c
HCC1954 Par
HCC1954 LR
HCC1954 NR
ECAR (mpH/min/mg total protein)
n.s.
Basal ECAR
Glycolytic capacity
Glycolytic reserve
Non-glycolytic acidification
d
SKBR3 Par
SKBR3 NR
SKBR3 TR
ECAR (mpH/min/mg total protein)
Basal ECAR
Glycolytic capacity
Glycolytic reserve
Non-glycolytic acidification
e
HCC1954 Par
HCC1954 LR
HCC1954 NR
OCR/ECAR (A.U.)
Basal
Maximum
f
SKBR3 Par
SKBR3 NR
SKBR3 TR
OCR/ECAR (A.U.)
Basal
Maximum

Figure 5

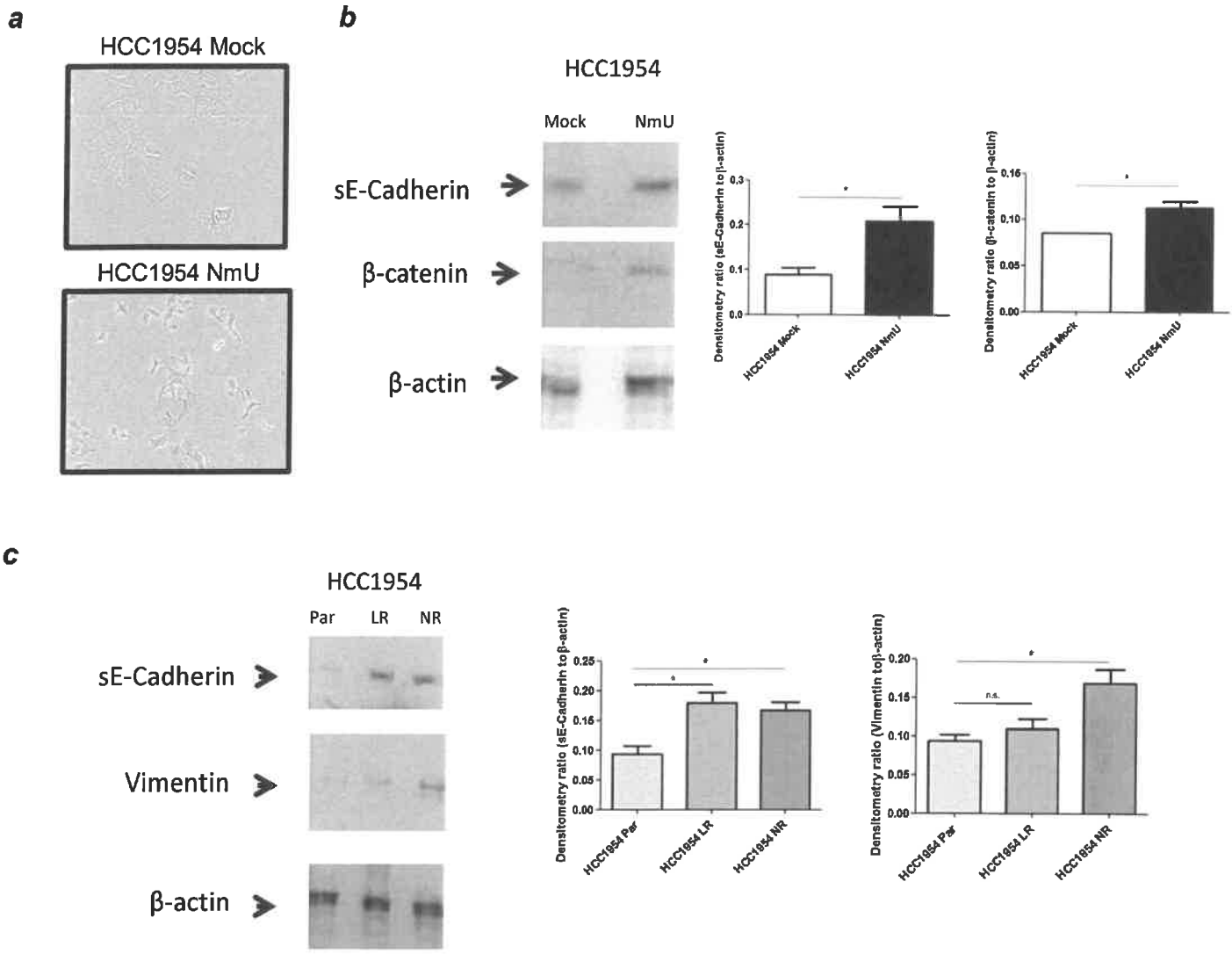
a
HCC1954 Mock
HCC1954 NmU
b
HCC1954
Mock
NmU
sE-Cadherin
β-catenin
β-actin
Densitometry ratio (sE-Cadherin to β-actin)
HCC1954 Mock
HCC1954 NmU
Densitometry ratio (β-catenin to β-actin)
HCC1954 Mock
HCC1954 NmU
c
HCC1954
Par
LR
NR
sE-Cadherin
Vimentin
β-actin
Densitometry ratio (sE-Cadherin to β-actin)
HCC1954 Par
HCC1954 LR
HCC1954 NR
Densitometry ratio (Vimentin to β-actin)
n.s.
HCC1954 Par
HCC1954 LR
HCC1954 NR

Figure 6

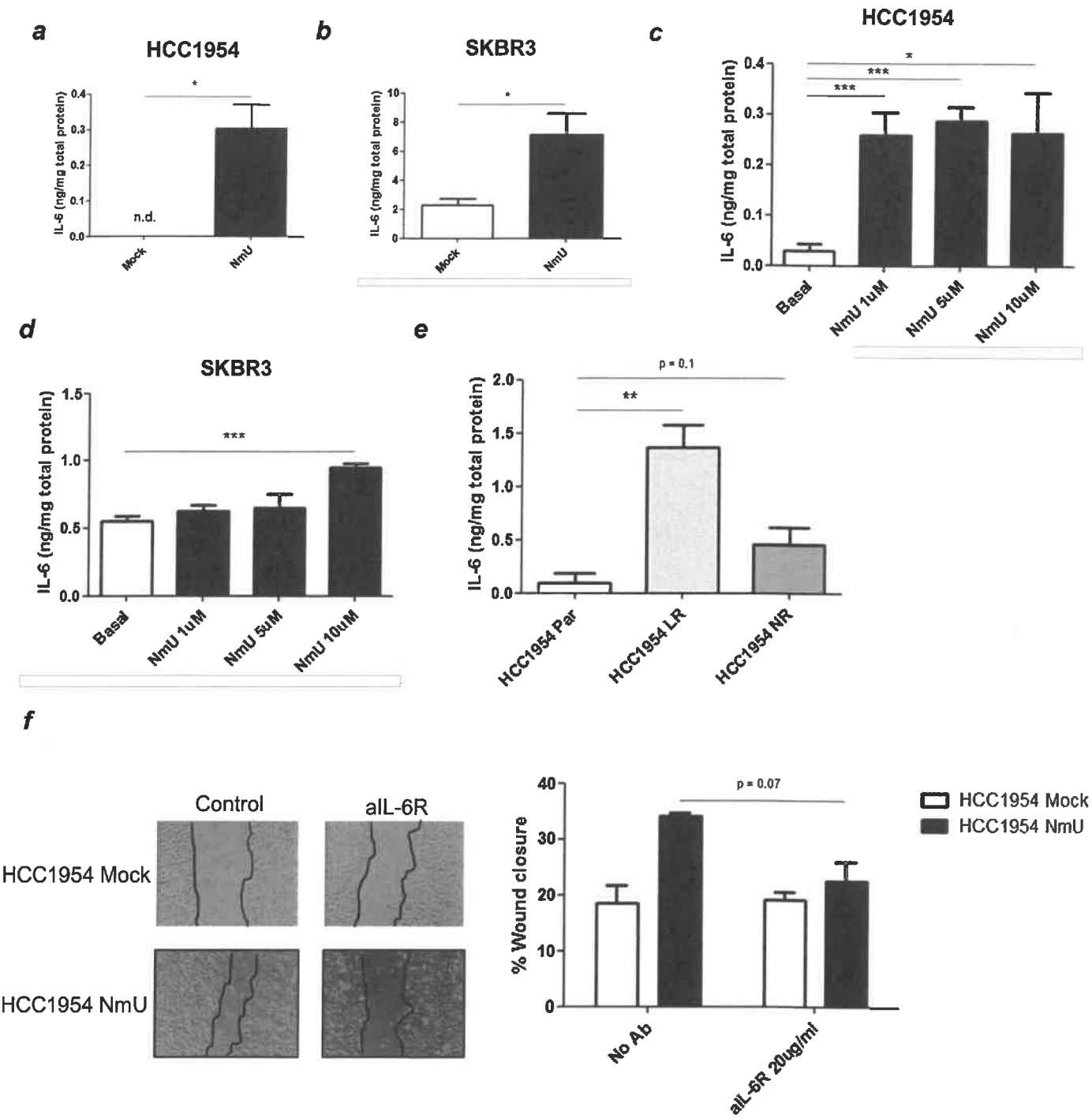
a
HCC1954
IL-6 (ng/mg total protein)
n.d.
Mock
NmU
b
SKBR3
IL-6 (ng/mg total protein)
Mock
NmU
c
HCC1954
IL-6 (ng/mg total protein)
Basal
NmU 1uM
NmU 5uM
NmU 10uM
d
SKBR3
IL-6 (ng/mg total protein)
Basal
NmU 1uM
NmU 5uM
NmU 10uM
e
p = 0.1
IL-6 (ng/mg total protein)
HCC1954 Par
HCC1954 LR
HCC1954 NR
f
Control
aIL-6R
HCC1954 Mock
HCC1954 NmU
% Wound closure
p = 0.07
No Ab
aIL-6R 20ug/ml
HCC1954 Mock
HCC1954 NmU

Figure 7

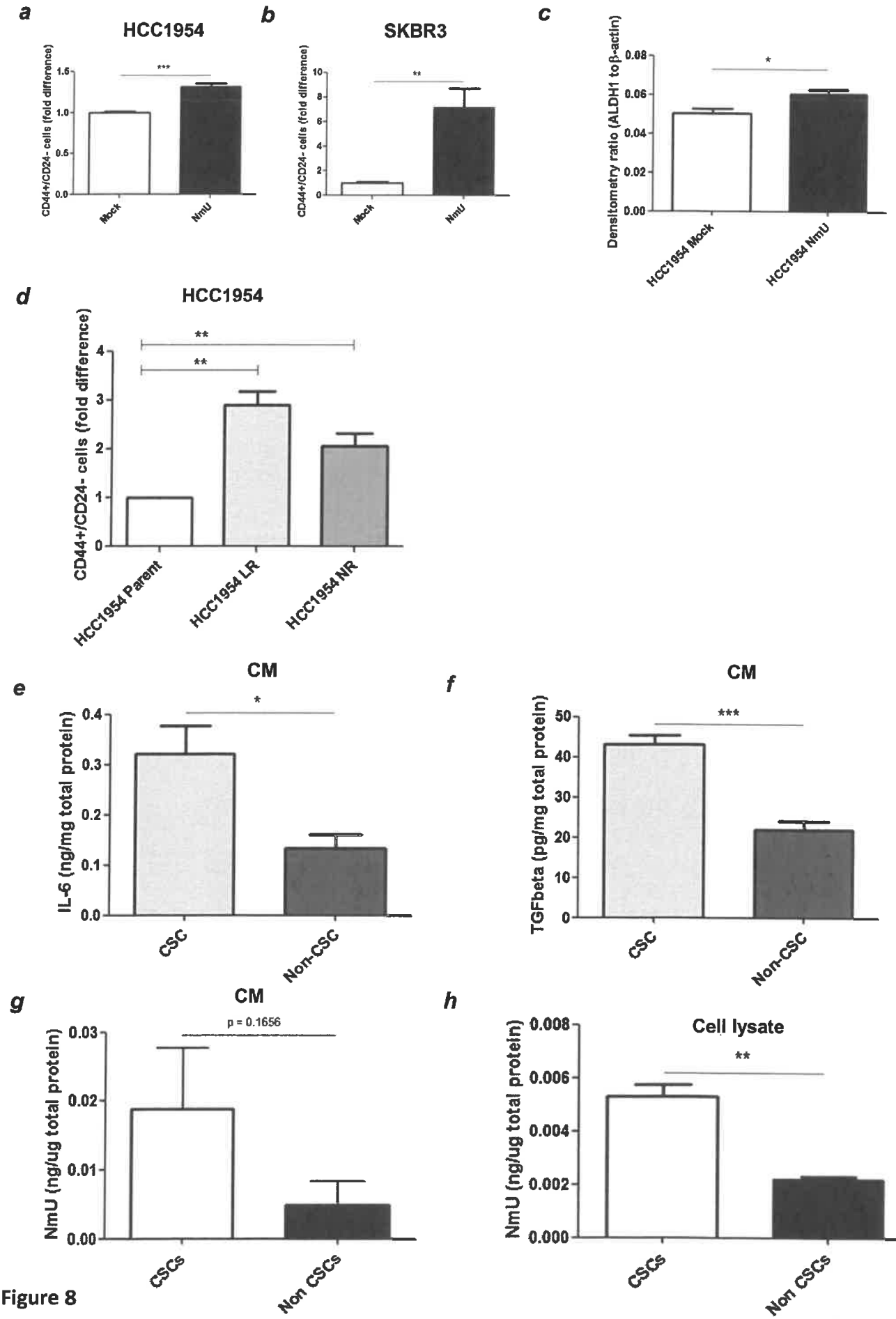
a
HCC1954
CD44+/CD24- cells (fold difference)
***
Mock
NmU
b
SKBR3
CD44+/CD24- cells (fold difference)
**
Mock
NmU
c
Densitometry ratio (ALDH1 to β-actin)
*
HCC1954 Mock
HCC1954 NmU
d
HCC1954
CD44+/CD24- cells (fold difference)
**
**
HCC1954 Parent
HCC1954 LR
HCC1954 NR
e
CM
IL-6 (ng/mg total protein)
*
CSC
Non-CSC
f
CM
TGFbeta (pg/mg total protein)
***
CSC
Non-CSC
g
CM
p = 0.1656
NmU (ng/ug total protein)
CSCs
Non CSCs
h
Cell lysate
NmU (ng/ug total protein)
**
CSCs
Non CSCs

Figure 8

a

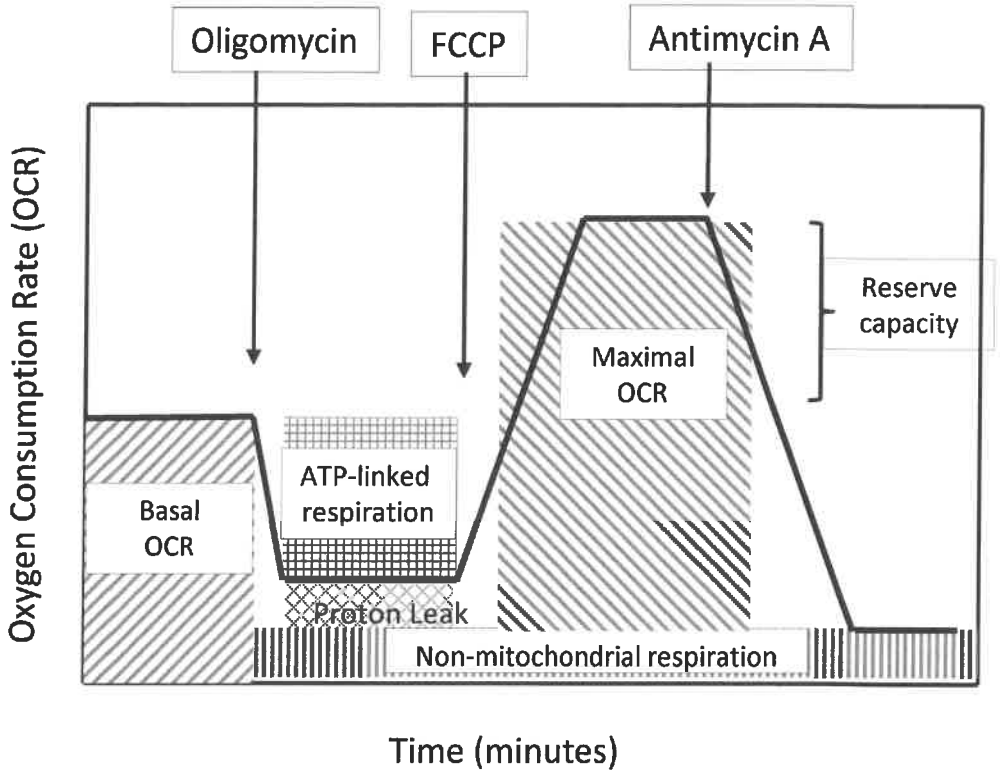

b

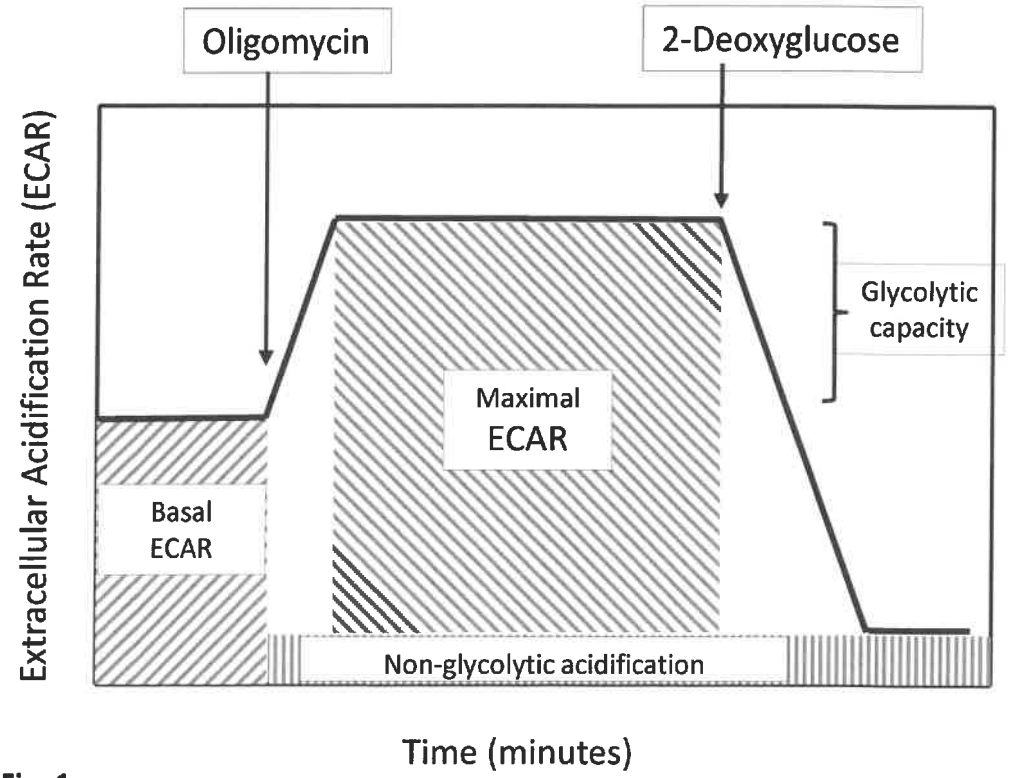

Suppl. Fig. 1

a

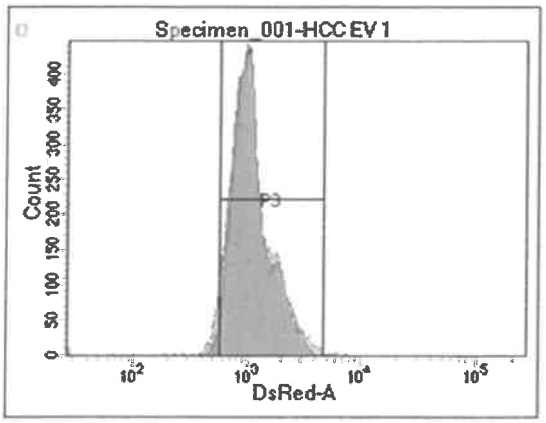

HCC1954 Mock

HCC1954 NmU

b

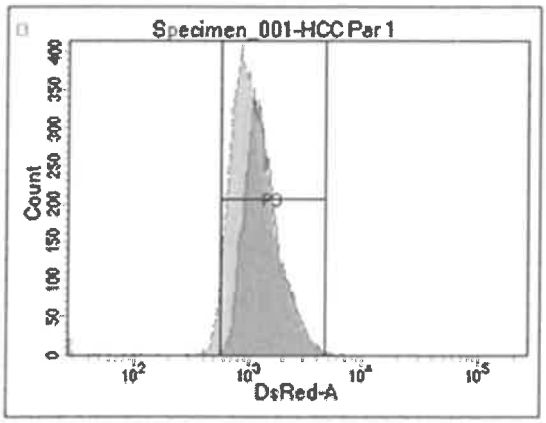

HCC1954 Par

HCC1954 LR

c

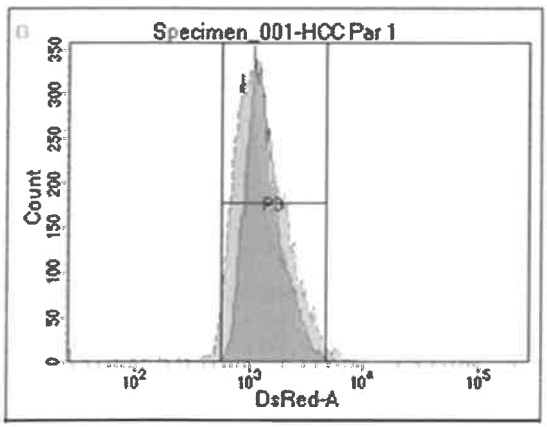

HCC1954 Par

HCC1954 NR

Suppl. Fig. 2

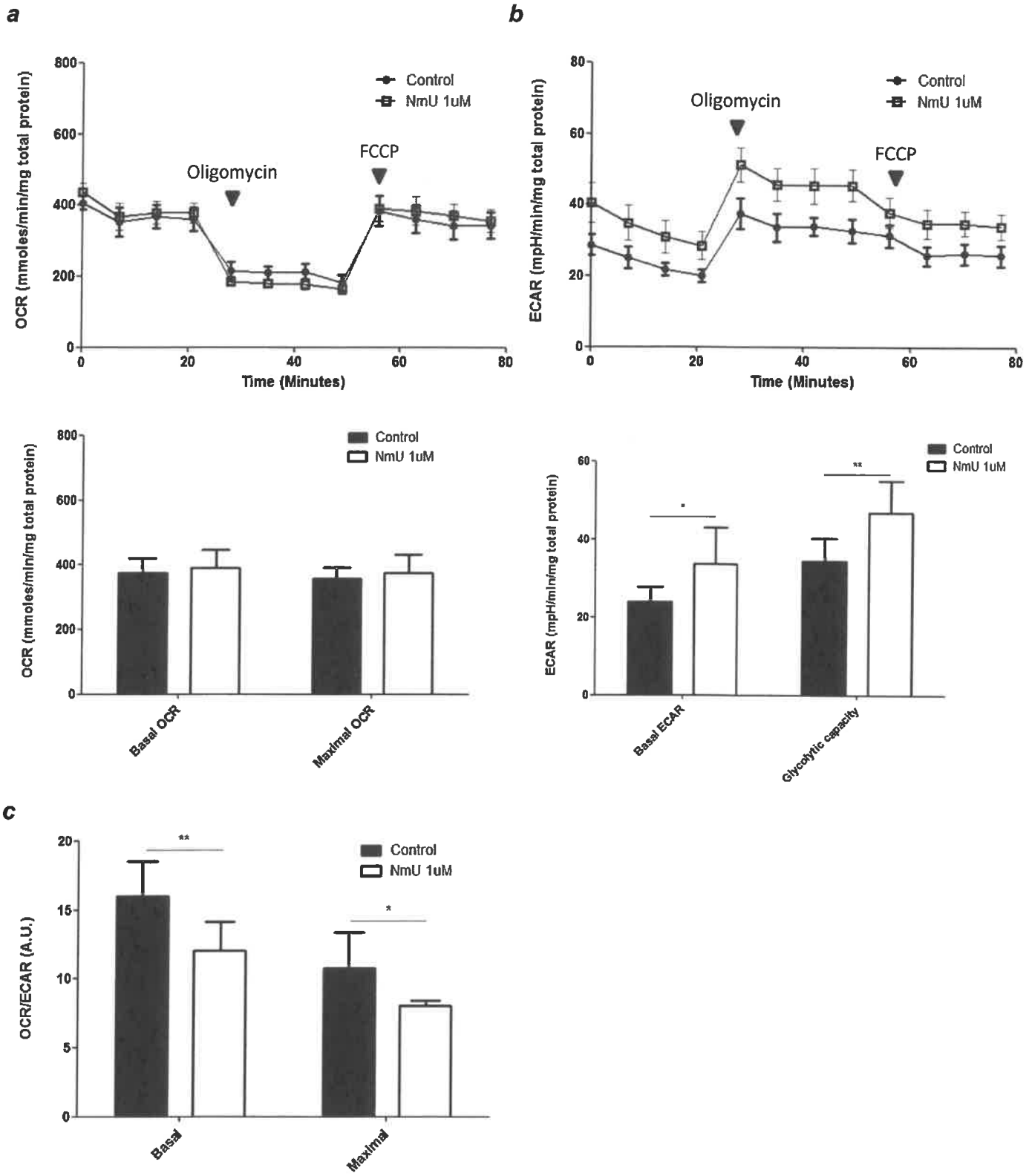
a
b
OCR (mmoles/min/mg total protein)
Control
NmU 1uM
Oligomycin
FCCP
Time (Minutes)
ECAR (mpH/min/mg total protein)
Basal OCR
Maximal OCR
Basal ECAR
Glycolytic capacity
c
OCR/ECAR (A.U.)
Basal
Maximal

Suppl. Fig. 3

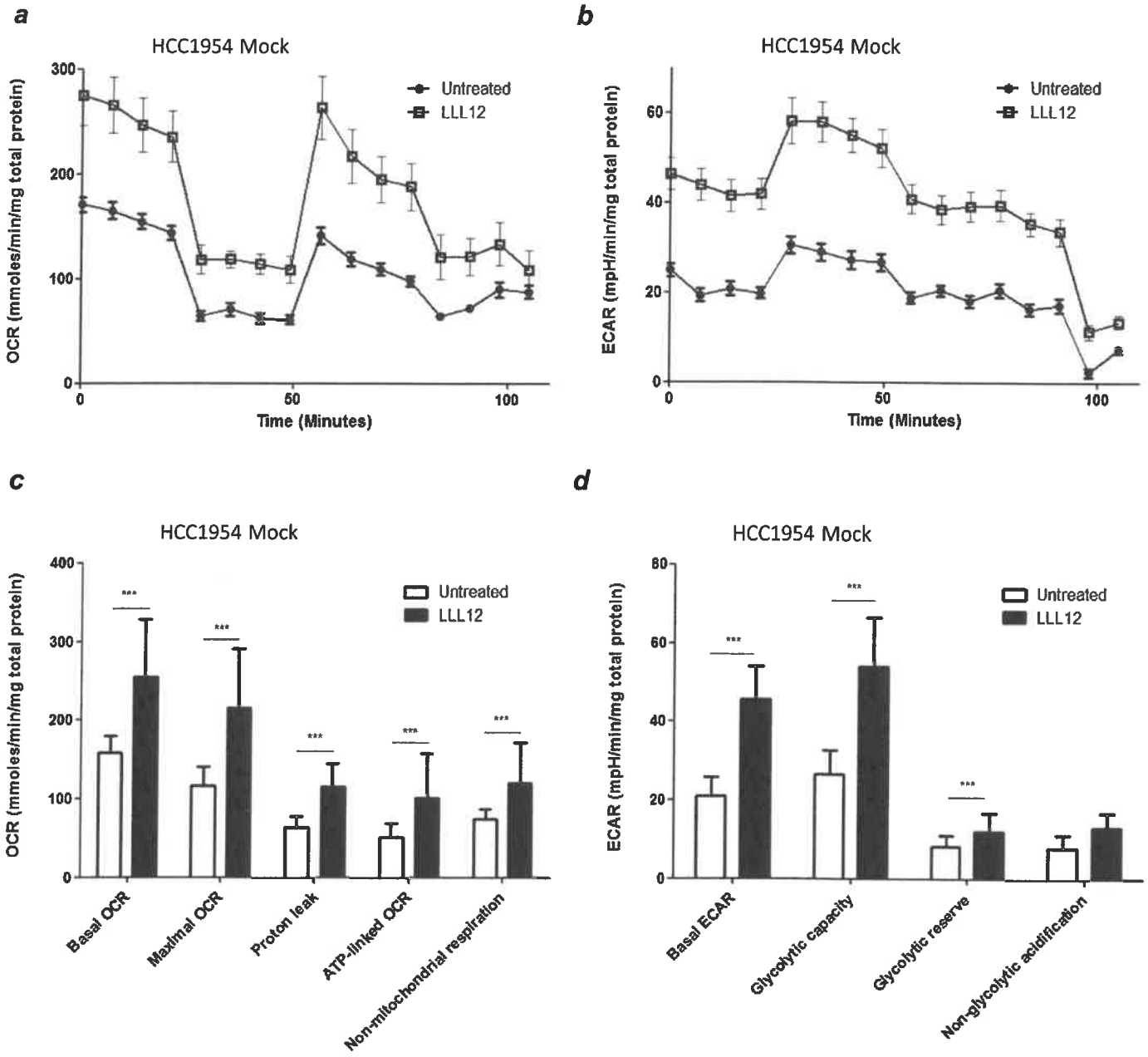
a
HCC1954 Mock
OCR (mmoles/min/mg total protein)
Untreated
LLL12
Time (Minutes)
b
HCC1954 Mock
ECAR (mpH/min/mg total protein)
Untreated
LLL12
Time (Minutes)
c
HCC1954 Mock
OCR (mmoles/min/mg total protein)
Untreated
LLL12
Basal OCR
Maximal OCR
Proton leak
ATP-linked OCR
Non-mitochondrial respiration
d
HCC1954 Mock
ECAR (mpH/min/mg total protein)
Untreated
LLL12
Basal ECAR
Glycolytic capacity
Glycolytic reserve
Non-glycolytic acidification

Suppl. Fig. 4

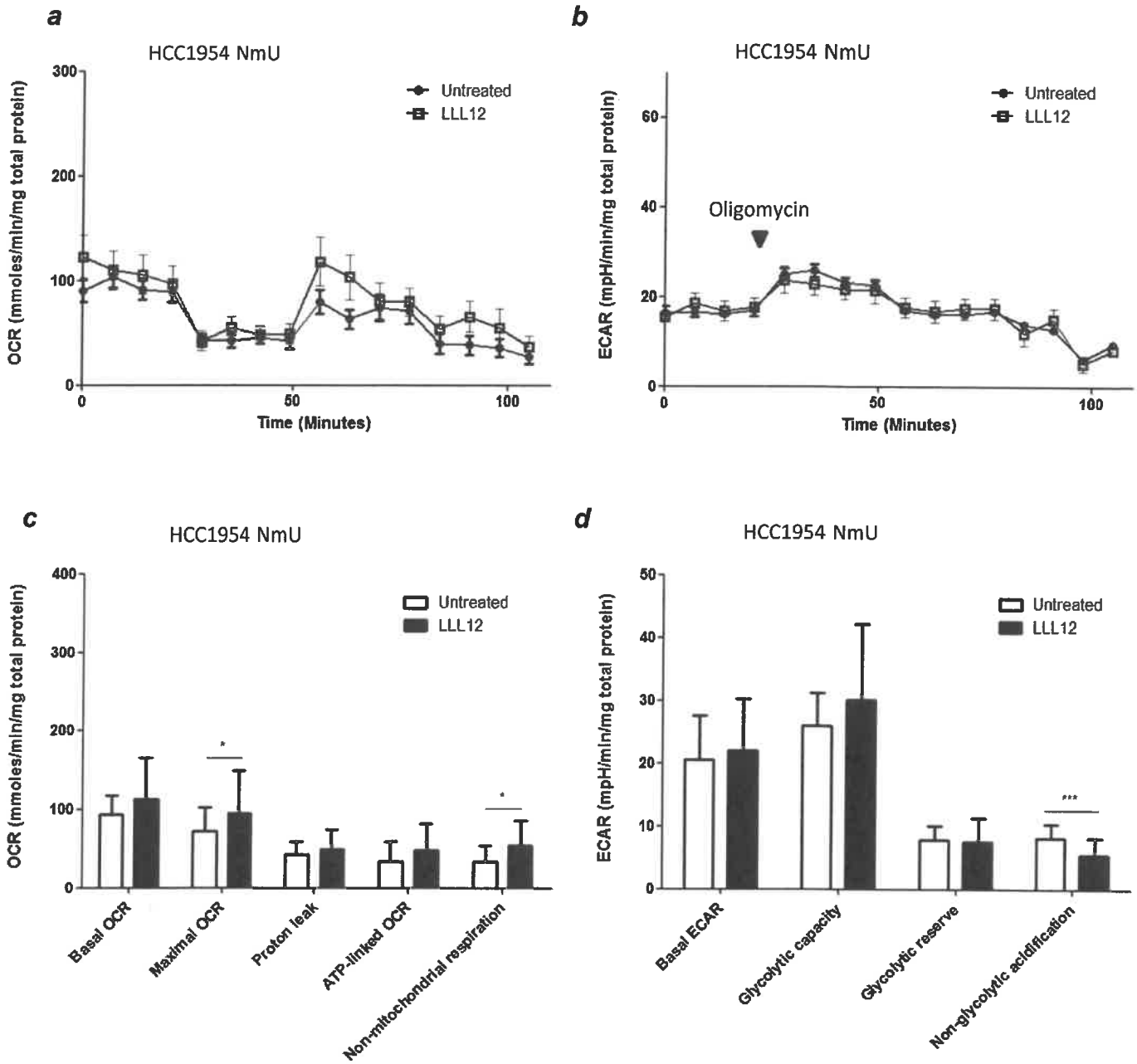
a
HCC1954 NmU
OCR (mmoles/min/mg total protein)
Untreated
LLL12
Time (Minutes)
b
HCC1954 NmU
ECAR (mpH/min/mg total protein)
Oligomycin
Untreated
LLL12
Time (Minutes)
c
HCC1954 NmU
OCR (mmoles/min/mg total protein)
Untreated
LLL12
Basal OCR
Maximal OCR
Proton leak
ATP-linked OCR
Non-mitochondrial respiration
d
HCC1954 NmU
ECAR (mpH/min/mg total protein)
Untreated
LLL12
Basal ECAR
Glycolytic capacity
Glycolytic reserve
Non-glycolytic acidification

Suppl. Fig. 5

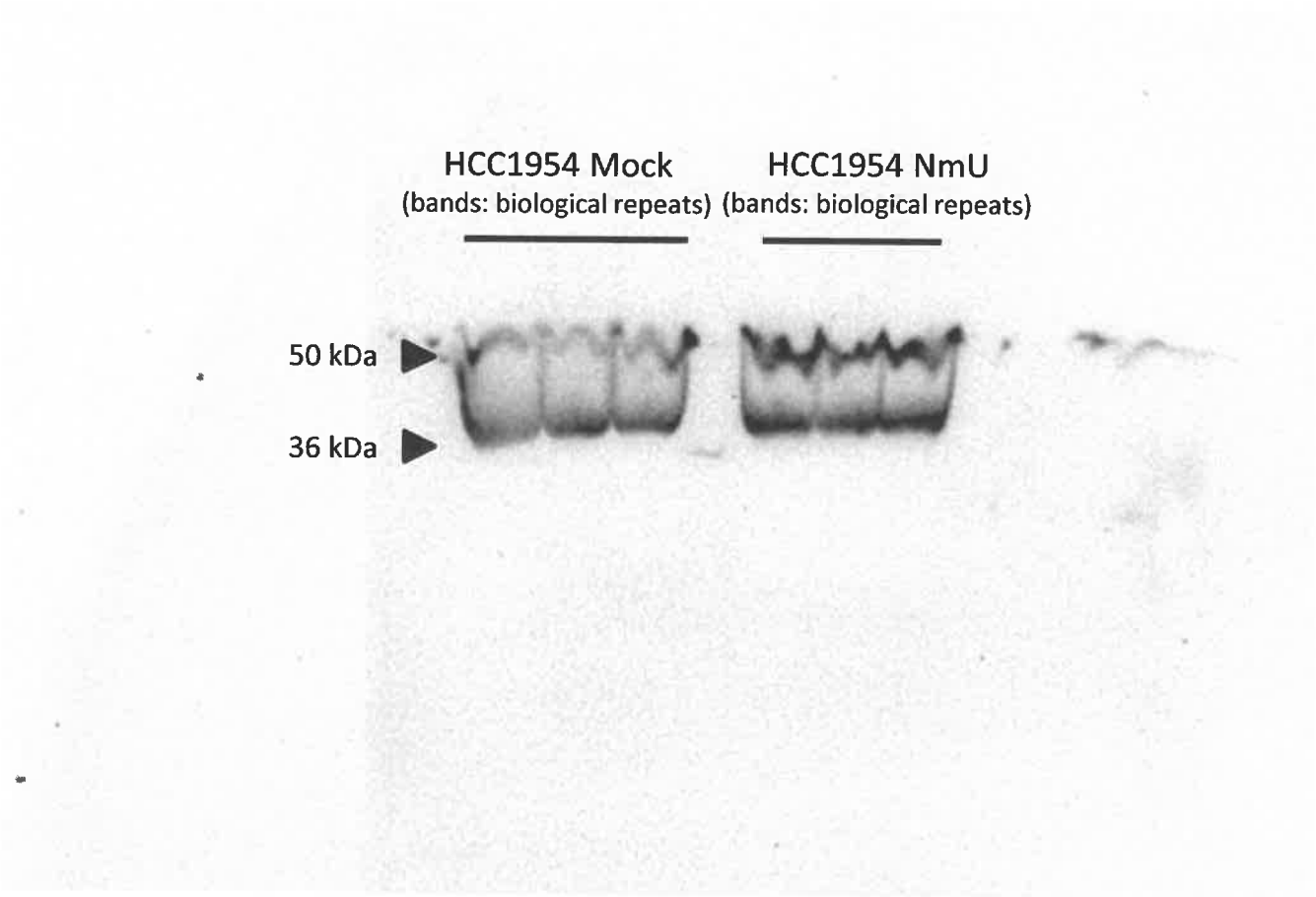
HCC1954 Mock
(bands: biological repeats)
HCC1954 NmU
(bands: biological repeats)
50 kDa
36 kDa

Suppl. Fig. 6